STRUCTURAL SYSTEMS
RESEARCH PROJECT

Report No.
SSRP – 2003/11

ELECTRICAL SUBSTATION EQUIPMENT INTERACTION – EXPERIMENTAL RIGID CONDUCTOR STUDIES

by

Christopher Stearns

André Filiatrault

Final Report to the Pacific Earthquake Engineering Research Center (PEER) for Task 402 of the PEER Lifeline Directed Studies Program

March 2004

Department of Structural Engineering
University of California, San Diego
La Jolla, California 92093-0085

University of California, San Diego
Department of Structural Engineering
Structural Systems Research Project

Report No. SSRP-2003/11

ELECTRICAL SUBSTATION EQUIPMENT INTERACTION – EXPERIMENTAL RIGID CONDUCTOR STUDIES

by

Christopher Stearns

Undergraduate Student Researcher

André Filiatrault

Formerly Professor of Structural Engineering

Department of Structural Engineering
University of California, San Diego
La Jolla, California 92093-0085

March 2004

DISCAIMER

Opinions, findings, conclusions and recommendations expressed in this report are those of the authors and do not necessarily reflect views of the Pacific Earthquake Engineering Research Center (PEER).

ACKNOWLEDGEMENTS

This project was sponsored by the Pacific Earthquake Engineering Research Center's Program of Applied Earthquake Engineering Research of Lifeline Systems supported by the California Energy Commission, California Department of Transportation, and the Pacific Gas & Electric Company.

This work made use of Earthquake Engineering Research Centers Shared Facilities supported by the National Science Foundation under Award Number EEC-9701568.

We greatly appreciated the input and coordination provided by Dr. Michael Riemer from PEER and Mr. Eric Fujisaki from the Pacific Gas and Electric Company (PG&E) during the development of this research project. The supports of Mr. David Chambers from the California Energy Commission and of Mr. Craig Riker from the San Diego Gas and Electric Company (SDG&E) are also gratefully acknowledged.

The authors acknowledge also Deutsch Power Products, Dossert Corporation and SDG&E for providing the test specimens considered in the experimental investigation.

TABLE OF CONTENTS

LIST OF SYMBOLS

a_c Horizontal acceleration measured at top of an equipment item

a_u Horizontal acceleration measured at top of equipment during an uncoupled seismic test

$E_{D\delta}$ Energy dissipated per cycle at displacement amplitude δ

F_δ Force at the displacement amplitude δ

F_c Force measured by load cell at top of equipment item during a coupled seismic test

F_{nh} Net horizontal force developed during a coupled seismic test

F_u Force measured by load cell at top of an equipment item during an uncoupled seismic test

m_{lc} Equivalent load cell mass

δ Displacement

δ_y Yield Displacement in ATC-24 loading protocol

$\mu\varepsilon$ Microstrain

μ Displacement ductility factor in ATC-24 loading protocol

ζ Equivalent viscous damping ratio

LIST OF FIGURES

LIST OF TABLES

1. INTRODUCTION

Electrical substation systems are used in virtually every locality of the United States to distribute electricity to local housing, hospitals, factories, and many other facilities. Earthquakes in recent years have demonstrated that these substations display a certain level of vulnerability to seismic loading (Benuska 1990, Hall 1995). Because substation equipment items were designed in the 1950s and 1960s, consequences from seismic events were not always taken into consideration. Certain components of these equipment were designed solely to supply electricity and have shown to perform poorly in seismic events. In response to these vulnerabilities, in recent years, the IEEE 693 standard (IEEE 1997) was developed to address the performance of substation equipment under seismic loading. However, this standard does not address the influence of interconnection on the equipment performance. Due to the complexity of the connectors, the seismic response of interconnected system may become complicated and unpredictable. Currently, according to the IEEE 693 standard, the equipments are qualified in a “stand-alone” condition.

One type of connection that is particularly complicated is the rigid bus connection. Typically, rigid buses utilize relatively flexible end connectors that account for thermal expansion. Examples of these types of connectors are shown in Figure 1.1. Depending on the flexibility and damping characteristics of these connectors, some of the seismic energy may be absorbed in the connectors before being transferred to the equipment components. Connectors in current systems, however, have shown not to provide a sufficient amount of flexibility nor dissipate a large amount of energy, thereby transferring forces to the equipment, resulting in damage.

Figure 1.1 Typical Rigid Bus Connectors

In 1999 as part of the Task 2C project of the PEER-PG&E program, several types of rigid bus connectors currently installed in electrical substations underwent quasi-static and shake table testing at the Charles Lee Powell Structural Systems Laboratories at the University of California, San Diego (Filiatrault et al., 1999). Three types of flexible strap connectors, which dissipate energy through yielding of and

friction between flexible straps, were tested. Additionally, a second type of connector, the bus slider connector, was tested. This bus slider dissipates energy through friction and exhibits a higher damping capacity. While the results of these tests showed a relatively good energy dissipation capacity, these connectors were relatively stiff and could transmit significant forces to the equipment. Consequently, these results led to the realization that connectors with lower stiffness should be examined as possible replacements for the current connectors.

This research project is the continuation of the investigation on substation equipment interaction performed in Task 2C of the PEER-PG&E program (Filiatrault et al., 1999). Two new specimens were recently fabricated to improve the connector performance through lower stiffness and higher damping capabilities. The primary objective of this report is to investigate experimentally the structural dynamic interaction between components of electrical substation equipment interconnected by these improved rigid bus connectors. The goal is to generate data such that a quantitative comparison can be made between the new connector specimens and the connectors currently used in substations, and to provide guidance for the implementation of the new connectors in current substations.

1.1 SCOPE OF RESEARCH

The main objective of the research is to experimentally investigate the interaction between components of substation equipment connected by re-designed (or improved) rigid bus connectors through quasi-static and shake table testing. The purpose was to generate data that would provide guidance in the design of conductor assemblies with

the improved connectors. Furthermore, another objective was to provide experimental validation data for a current PEER-PG&E project in which analytical studies are being conducted at the University of California, Berkeley. Specific tests conducted in this project were:

(i) Full-scale quasi-static cyclic tests of one improved flexible strap connector.

(ii) Full-scale quasi-static cyclic tests of one improved rigid bus slider.

(iii) Full-scale shake table tests of five different pairs of generic substation equipment connected with three different improved rigid bus assemblies.

The seismic testing in this project was conducted on a uniaxial shake table. Although this could be considered a limitation because of the multi-directional input of earthquake ground motions, limiting the excitation in the axial direction of the bus assemblies allows the validation of analytical studies in the most damaging axial input direction without introducing supplemental variables from other shaking directions.

1.2 REPORT LAYOUT

The following report is divided into six chapters. **Chapter one** presents an introduction to the project, and scope of the current study. **Chapter two** describes the quasi-static tests performed on the flexible strap connector and bus slider. **Chapter three** presents the shake table tests performed on five pairs of generic substation equipment connected with three different rigid bus assemblies. **Chapter four** presents the results of the numerical modeling performed on several rigid bus assemblies using the computer program RUAUMOKO. **Chapter five** summarizes the results obtained and offers some conclusions. The references used for this report are then listed in

Chapter six. Finally, five appendices present shop drawings of the specimens followed by the detailed results from each shake table test conducted.

2. QUASI-STATIC TESTS OF RIGID BUS CONNECTORS

2.1 INTRODUCTION

This chapter describes the quasi-static tests performed on improved S-shaped Flexible Strap Connectors (S-FSC) and on an improved bus slider connector. These tests were performed in the longitudinal direction of the connectors under a prescribed displacement history. The main objective of these tests was to obtain the mechanical properties of each specimen and compare them with the mechanical properties of the connectors tested previously in the Task 2C study. The mechanical properties of the connectors are also used in the aid of the numerical modeling.

2.2 DESCRIPTION OF TEST SPECIMENS

2.2.1 S-FSC SPECIMENS

The first of two specimens provided by PG&E was the improved S-shaped flexible strap connector (S-FSC). As shown in Fig. 2.1a.), this recently proposed connector (Song 2004, Song et al. 2004) incorporates an anti-symmetrical geometry with two horizontal terminal pads. The three FSC specimens that were previously tested in Task 2C are shown in Fig. 2.1 b.) and are described as follows: the first FSC specimen (Part 30-2021) is non-symmetrical with one horizontal and one vertical terminal pad. The second FSC specimen (Part 30-2022) is symmetrical with two horizontal terminal pads. Finally, the third FSC specimen is non-symmetrical with two horizontal terminal pads at different elevations. The main differences between the

improved S-FSC specimen and the previous FSC specimens are longer length, and its S-shape design. Drawings of the specimens are included in Appendix A.

a.)

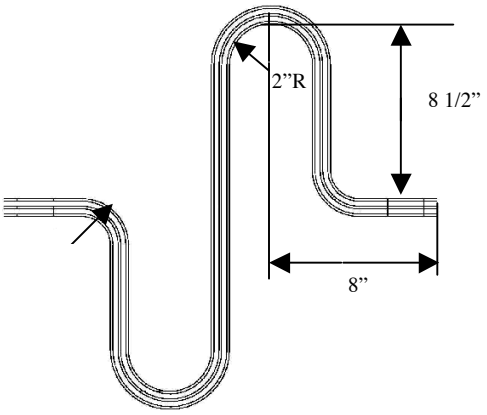

b.)

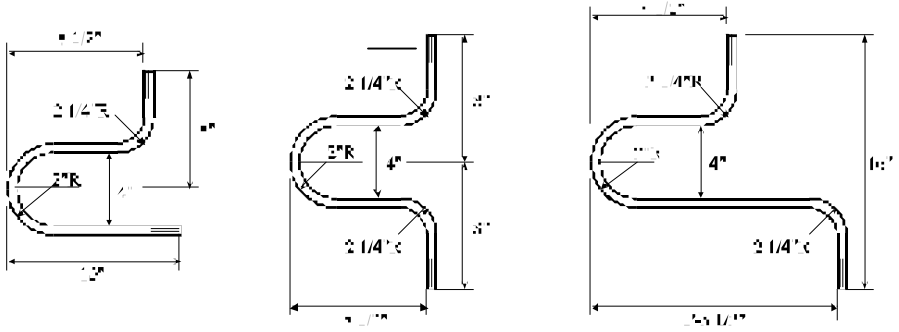

PG&E FSC No. 30-2021 PG&E FSC No. 30-2022 PG&E FSC No. 30-2023

Figure 2.1 Dimensions of FSC Specimens.
a.) S-Shape FSC (S-FSC) Specimen (Song 2004, Song et al. 2004)
b.) Previously Tested FSC Specimens

Each connector was made up of three pairs of copper alloy straps (1/8" thick by 3" wide) separated by two 1/4" gaps. Shim plates were inserted in the gaps only at the ends of the springs to provide continuous connection to the terminal pads (Filiatrault et al., 1999).

When the S-FSC specimen first arrived in the laboratory, it was in a compressed form, rather than the expected S-shape form. Figure 2.2 presents this mis-shaped

specimen. To return the specimen to the desired shape, each end was pulled apart a certain distance until a satisfactory shape was achieved. This new shape is also shown in the figure. Due to the extension of the specimen, yielding occurred in the straps and changed the properties of the specimen for the quasi-static test. Thereafter, another connector was manufactured in the correct shape. Quasi-static testing was then performed on both specimens. However, only the second specimen incorporating the correct initial geometry was used for the shake table tests.

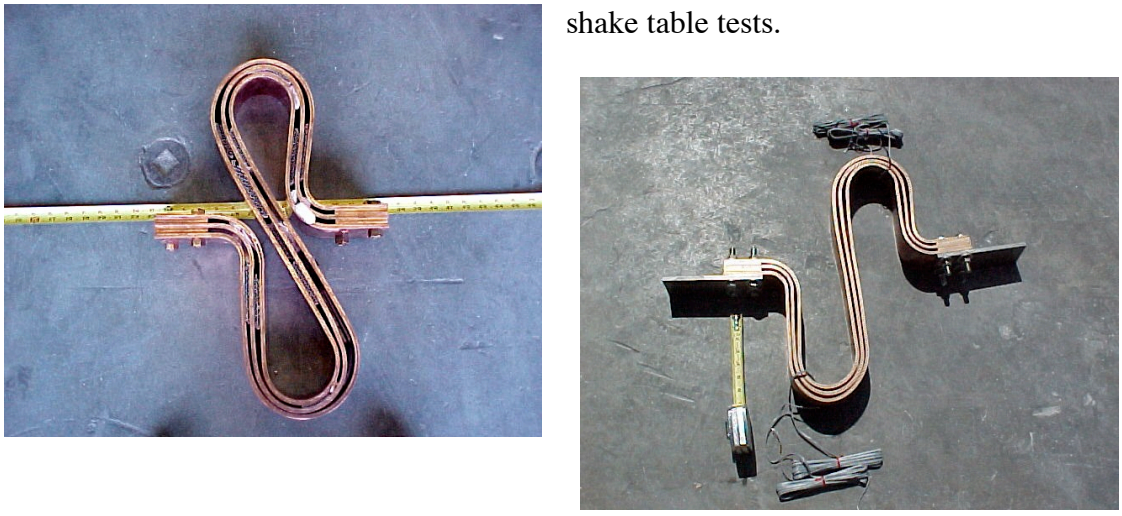

Figure 2.2 Initial and Final Shape of First (Mis-Shaped) S-FSC Specimen

2.2.2 BUS SLIDER SPECIMEN

The second specimen provided by PG&E was an improved bus slider connector. As shown in Fig. 2.3, the original bus slider specimen tested in Task 2C was designed such that there were two side-by-side aluminum cables on the top and bottom face of the tube (Filiatrault et al., 1999). At one end of the cables, terminal pads coupled the cables together. A sliding shaft was also attached at this point and would slide into the

tube when under compression, thereby creating a friction force against the inside surface of the pipe. It would then slide out from the tube under tension, utilizing the cables as the restoring force. The other end of the cables were simply welded to a point a certain distance down on the 10-ft long SPS aluminum pipe (4.5 in outside diameter and 4.026 in inside diameter).

The improved bus slider specimen had some important modifications from the previous one tested. Figure 2.3 shows a comparison between the two specimens. The first difference between the two specimens was the increased allowable stroke in the improved bus slider. The original specimen could only accommodate 3.5 in of displacement in both the compression and tension directions (7 in peak-to-peak), while the stroke on the improved specimen could accommodate 5 in (10 in peak-to-peak). One important note to point out is that the plunger fixture on the improved specimen was not completely centered when it arrived in the laboratory. As a result of the fabrication, 8 in of the plunger was outside of the tube, and only 2 in was inside of the tube in its resting position. Since both the quasi-static and shake table tests required maximum stroke in both directions, the specimen had to be compressed 3 in, resulting in an allowable stroke of 5 in. in both directions.

Another difference the improved bus slider specimen exhibited was the placement of the cables. The cables were spread out equally around the pipe. This may have been implemented to increase resistance to torsion. Another modification of the improved bus slider was the emancipation from the aluminum tube. Unlike the original specimen, the specimen was not welded to the tube. Instead, the design allowed for the tube to be inserted into the end of the connector. A compression fitting was then

required to provide a clamping force from the specimen onto the aluminum pipe, as shown in Figure 2.4. A final important modification made to the improved bus slider was the implementation of stoppers at the end of the plunger inside the tube. These stoppers were installed such that if the plunger were to be extended to the maximum 5 in stroke, the plunger would not fully slide out of the tube. There was no mechanism to prevent pull-out when the maximum stroke was reached on the original bus slider.

Original Bus Slider

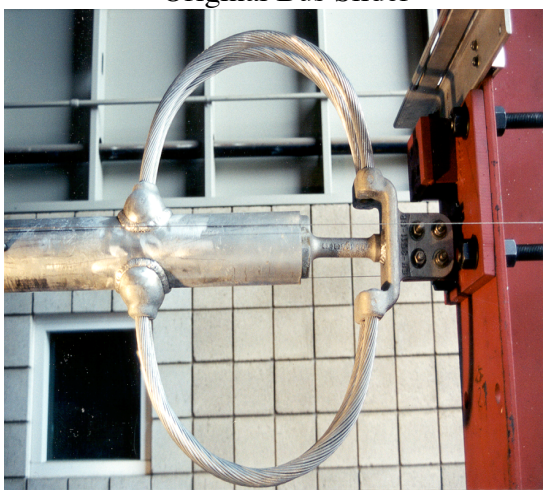

Improved Bus Slider

Figure 2.3 Slider Specimens

Figure 2.4 Bus Slider Compression Fitting

2.2.3 SEFCOR SPECIMEN

The third specimen investigated was manufactured by the SEFCOR company and was provided by San Diego Gas and Electric (SDG&E). This connector utilizes only two aluminum cables in a single loop configuration. It has one horizontal and one vertical terminal pad with an allowable stroke ranging from 24 in to 30 in. For testing purposes, the separation distance used was set at approximately 29 in. The SEFCOR specimen was received while the shake table tests were underway and after the quasi-static tests had been performed on the other specimens. For this reason, and because of time constraints, the SEFCOR connector did not undergo the quasi-static testing. Figure 2.5 presents a photograph of the SEFCOR connector.

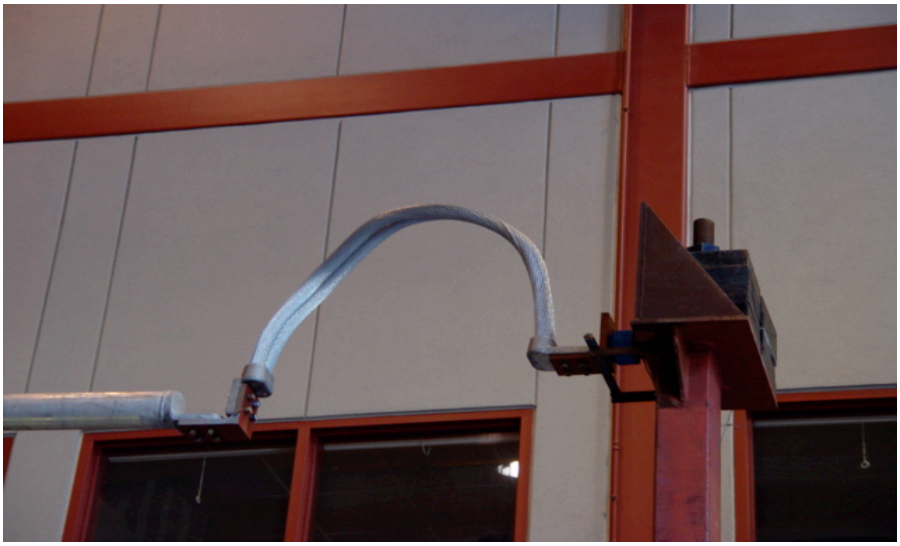

Figure 2.5 SEFCOR Connector

2.3 COPPER ALLOY PROPERTIES

In the Task 2C project (Filiatrault et al., 1999), monotonic tensile tests were performed on several coupons taken from the FSC specimen specimens in order to

evaluate the properties of the copper alloy. Three different coupons were tested according to the ASTM E8-98 standard (American Society for Testing Materials, 1999). The results of the tests showed that the alloy exhibited almost a perfect elastic-plastic behavior that can be characterized by a Young's Modulus and a yield strength. Table 2.1 presents these material properties based on the mean values of the three tests performed (Filiatrault et al., 1999).

Table 2.1 Material Properties for Copper Alloy (from Filiatrault et al., 1999)

Young's Modulus	14 100 ksi
Yield Strength	27 ksi
Yield Strain	1915 $\mu\varepsilon$

2.4 EXPERIMENTAL SET-UP FOR QUASI-STATIC TEST

Figure 2.6 illustrates the experimental set-up used to perform the quasi-static tests on the S-FSC specimens and on the bus slider. From the figure, it is clear that the bus slider has been compressed by the bulging of the cables. This was done to account for the 3 in offset as previously mentioned. In the configuration shown, the specimen has been properly centered and can accommodate 5 in. in both directions. In compressing the slider, however, a small force offset was observed.

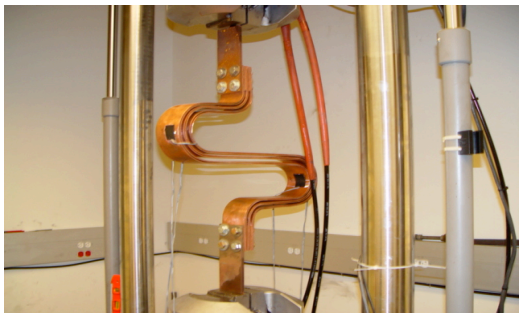

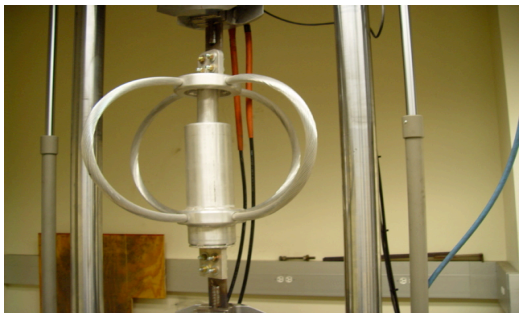

Figure 2.6 Experimental Set-Up for Quasi-Static Tests on Connectors

A 110-kip capacity MTS testing machine was used for the quasi-static tests. This machine can accommodate a displacement of 4 in. in both directions when completely centered. The 110-kip actuator is located on the bottom portion of the machine. This portion of the testing machine also displaces during the test, while the other segment remains stationary. To place the specimens into the machine for testing, several fixtures were fabricated. Four holes were drilled into two ¼" steel plates, each of which was bolted to an end of the specimen at the terminal pad. Then, a standard #3 rebar was welded to the opposite end of the steel plate, and this bar was inserted into the v-notched clamps of the testing machine. With this method, all fixtures remained rigid. Note also that the specimens were required to be placed into the machine in a vertical position, which is different from the horizontal direction used for the shake table tests.

2.5 INSTRUMENTATION

The force-displacement hysteresis loops were obtained by measuring the load across the 110-kip load cell and the displacement transducer of the MTS testing machine. For the bus slider specimen, only load and displacement were recorded for the quasi-static test. For the S-FSC specimen, load and displacement were obtained from the machine, and four strain gauges were also applied on each loop of the specimen. Figure 2.7 illustrates the strain gauge configuration on the specimen. These gauges were applied so that the strain could be monitored during the test to ensure that

the specimen would not reach the yielding strain of 1915 $\mu\varepsilon$. Strain gauges were applied on the upper and lower loop, one on the outside and one on the inside of the loop. The strain gauges are identified by the "SG" labels, numbered one through four.

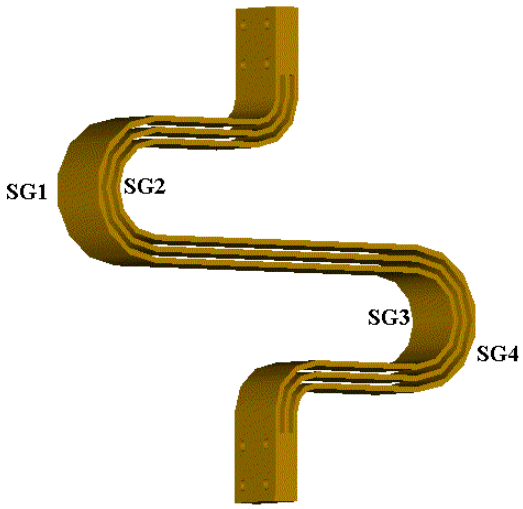

Figure 2.7 Strain Gauge Placement on S-FSC Specimen

2.6 TEST PROTOCOL

The loading protocol used to perform the cyclic tests was inspired by the ATC-24 loading protocol (Applied Technology Council, 1992). This protocol has been developed for the cyclic seismic testing of components of steel structures. As shown in Figure 2.8, the protocol consists of stepwise increasing displacement, δ, expressed in terms of a displacement ductility factor, μ, defined as:

$$\mu = \frac{\delta}{\delta_y} \tag{2.1}$$

An arbitrary value of 1 in was taken as the yield displacement, δ_y, across each of the specimens (Filiatrault and Stearns, 2003).

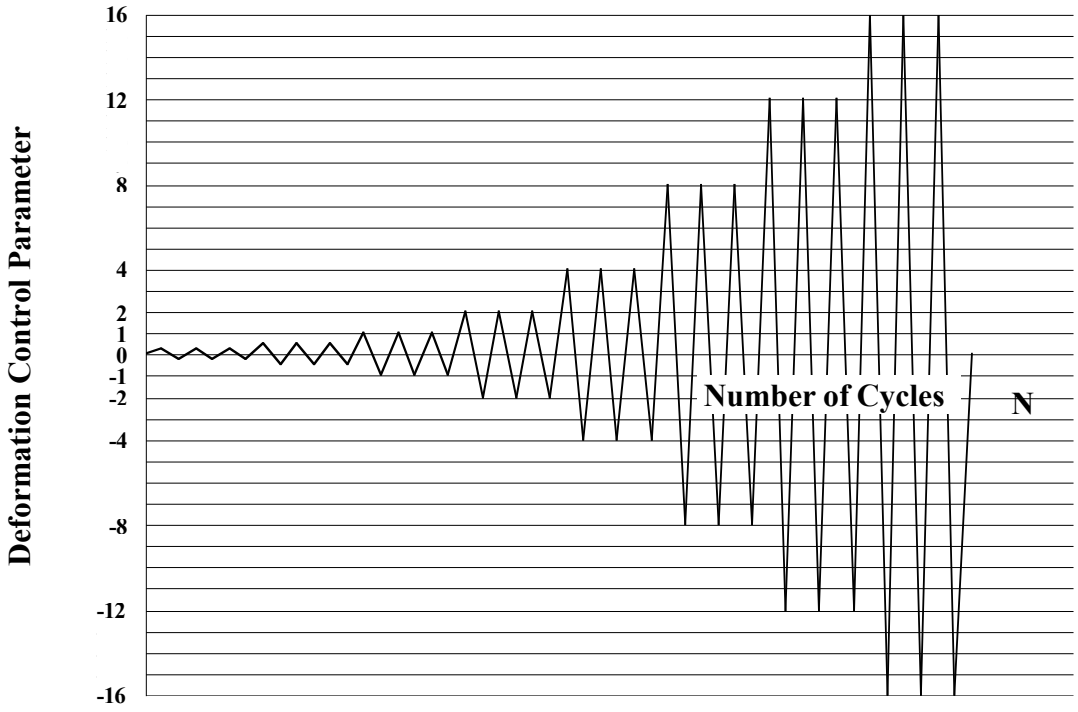

Figure 2.8 Loading Protocol for Quasi-Static Cyclic Tests

Due to the testing machine limitations, the maximum displacements reached by the machine were 4 in and -4 in.

2.7 EXPERIMENTAL RESULTS

2.7.1 FLEXIBLE STRAP CONNECTOR RESULTS

Figures 2.9 and 2.10 present photographs of each of the two S-FSC specimens under maximum compression and tension forces. The first S-FSC specimen was displaced by 4 in. in both directions. This caused yielding in the specimen. Because the specimen had previously been yielded in the process of re-shaping its geometry, it was decided that going beyond yield for the quasi-static test was acceptable. For the second S-FSC specimen, however, it was important to stay below yield since this

specimen would later be used for the shake table tests. For this reason, it was necessary to retain the initial properties. Consequently, during the test, the strain was monitored and was found to exceed the yield strain of 1915 $\mu\varepsilon$ for a displacement over 2 in. Therefore, the specimen was cycled to a maximum displacement of 2 in to prevent yielding.

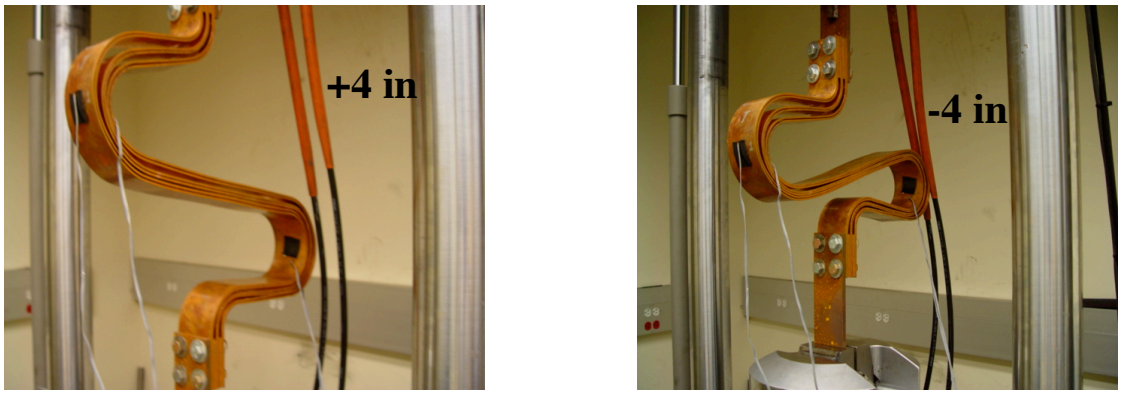

Figure 2.9 First (mis-shaped) S-FSC Specimen at Maximum Displacements

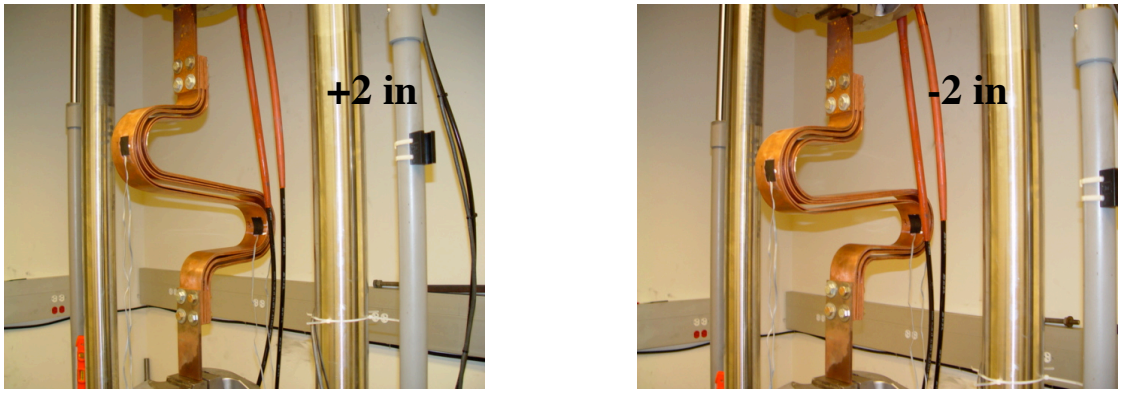

Figure 2.10 Second S-FSC Specimen at Maximum Displacements

Figure 2.9 clearly shows the asymmetrical shape at the maximum displacements of the re-shaped S-FSC specimen. This was caused by the nature of the looped regions. Due to the re-shaping of the connector in the looped regions, the straps tended to pinch together, creating friction. Due to this influence and the previous yielding, fat

hysteresis loops resulted. The second S-FSC specimen exhibited a similar stiffness but with a thinner hysteresis loop. Figure 2.11 shows a comparison of the hysteresis loops measured on both specimens.

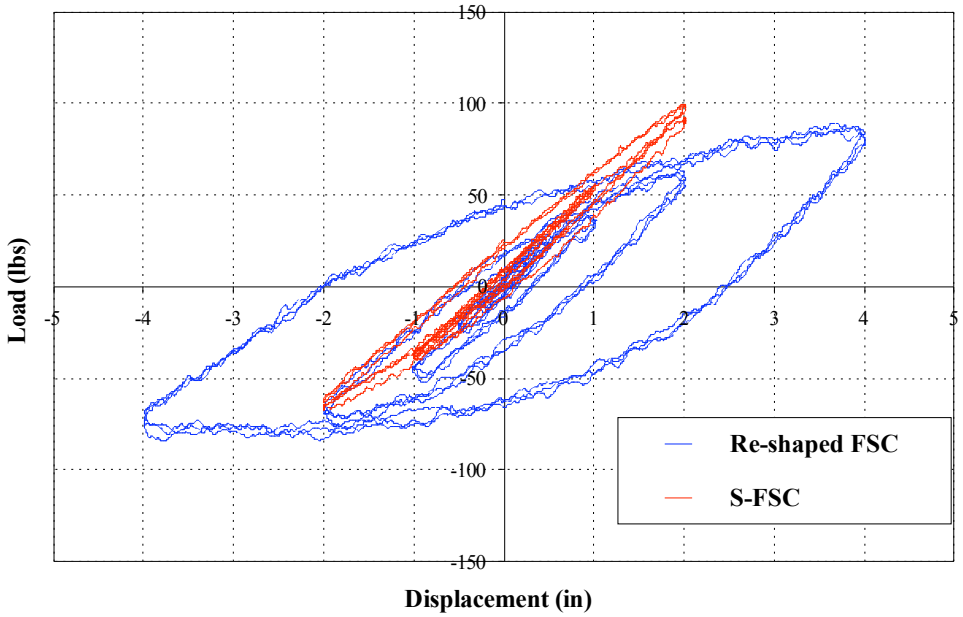

Figure 2.11 Flexible Strap Connector Hysteresis Loops

From the figure, the differences between the two specimens are clear. When examining the linear regions of both specimens, which can be seen at the 2 in displacement cycles, the second specimen displays slightly higher forces with a thinner loop. However, despite these differences, the stiffness of each specimen at this level was consistent. The secant stiffness of the first specimen at the 2 in displacement was 35.5 lbs/in, while the secant stiffness of the second specimen was 41.0 lbs/in.

When considering the initial stiffness of each connector, it is necessary to examine the initial linear portion of the load-displacement plot. Each of the three FSC specimens previously tested in Task 2C (Filiatrault et al., 1999) were displaced

through the same ATC-24 loading protocol. Figure 2.12 compares the load-displacement curves for the three previously tests FSC specimens with that of the S-FSC specimen. In the figure, only the results of the second S-FSC specimen, incorporating the correct initial geometry, are presented.

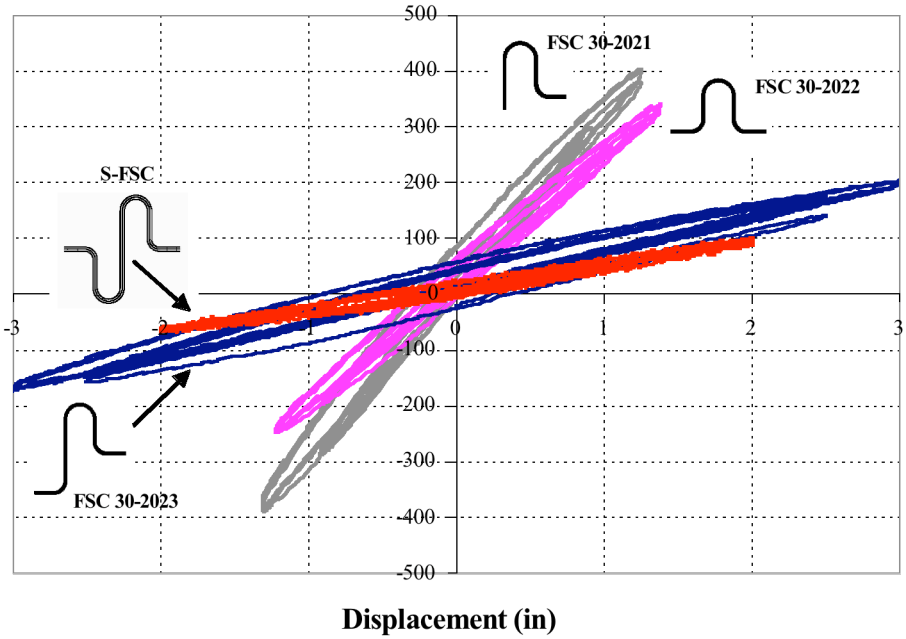

Figure 2.12 Flexible Strap Connector Hysteresis Loops

The figure shows that the S-FSC specimen has the lowest initial stiffness compared to the other three specimens. Table 2.2 summarizes the initial stiffness properties for all four tested specimens. The maximum loads and displacements obtained from the tests are also tabulated. For the initial stiffness, a trend line was applied to the load-displacement data for each specimen to obtain an average stiffness. The results from this data show that the initial stiffness of the S-FSC was approximately two-thirds of that of FSC 30-2023, the most flexible of the three previously tested FSC specimens.

Table 2.2 Initial Stiffness of Flexible Strap Connectors.

Connector	Absolute Maximum Displacement (in)	Absolute Maximum Force (lbs)	Initial Stiffness (lbs/in)
FSC 30-2021	1.31	403.9	307.8
FSC 30-2022	1.38	339.4	226.8
FSC 30-2023	3.01	202.8	61.9
S-FSC	2.00	103.0	41.0

During the cyclic loading of specimens such as these, as the displacements are incrementally increased, the secant stiffness at each amplitude may decrease because of inelastic behavior. Therefore, it is necessary to examine the trend of change in secant stiffness of the specimens with increasing displacement. This secant stiffness can be determined by taking the slope of the line from the origin to the maximum point of the load-displacement curve. This was then done for each displacement amplitude at which the specimens were cycled. Figure 2.13 presents the comparison of the secant stiffness of the four FSC specimens tested. Again, from the figure, it is clear that the S-FSC displays the lowest secant stiffness.

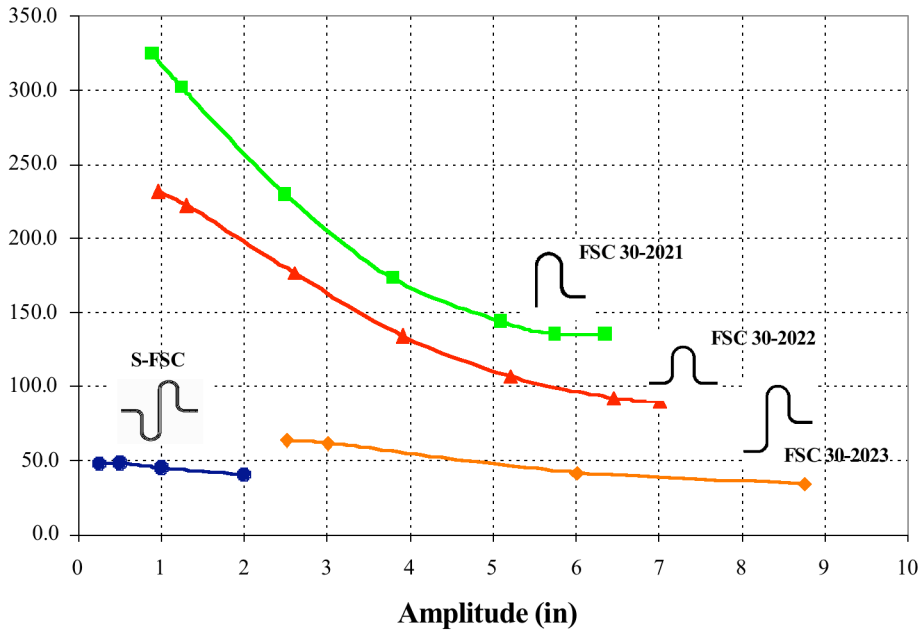

Figure 2.13 Secant Stiffness of FSC Specimens

2.7.2 BUS SLIDER CONNECTOR RESULTS

The ATC-24 loading protocol was again applied to the bus slider previously tested in Task 2C. However, in this instance, the yield displacement was defined differently since Coulomb-type friction was governing the nonlinear behavior (Filiatrault et al., 1999). Consequently, the displacement amplitudes at which the specimen was cycled were 1 in, 2 in and 3 in, respectively. For the improved bus slider, however, the displacement amplitudes of 0.25 in, 0.5 in, 1 in, 2 in, and 4 in used for the S-FSC specimens were applied also. Figure 2.14 presents the photographs of the improved bus slider specimen at maximum displacements. Since the improved bus slider could accommodate a displacement of 5 in, the maximum amplitude of 4 in was acceptable.

Figure 2.15 presents the load-displacement response of both bus slider specimens. Both specimens exhibit a behavior that is typical of a Coulomb-type friction system coupled with an elastic restoring force mechanism. Before the slider can move, the static friction between the shaft and the interior surface of the pipe must be overcome.

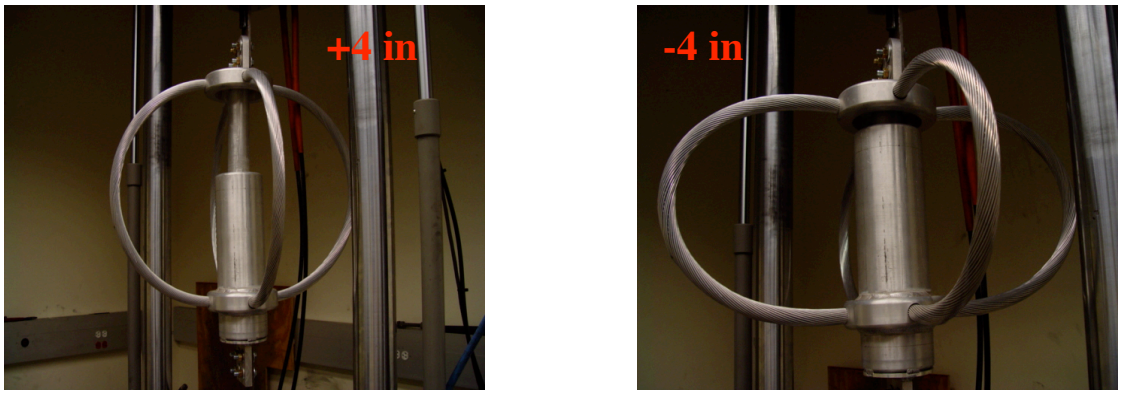

Figure 2.14 Bus Slider Specimen at Maximum Displacements

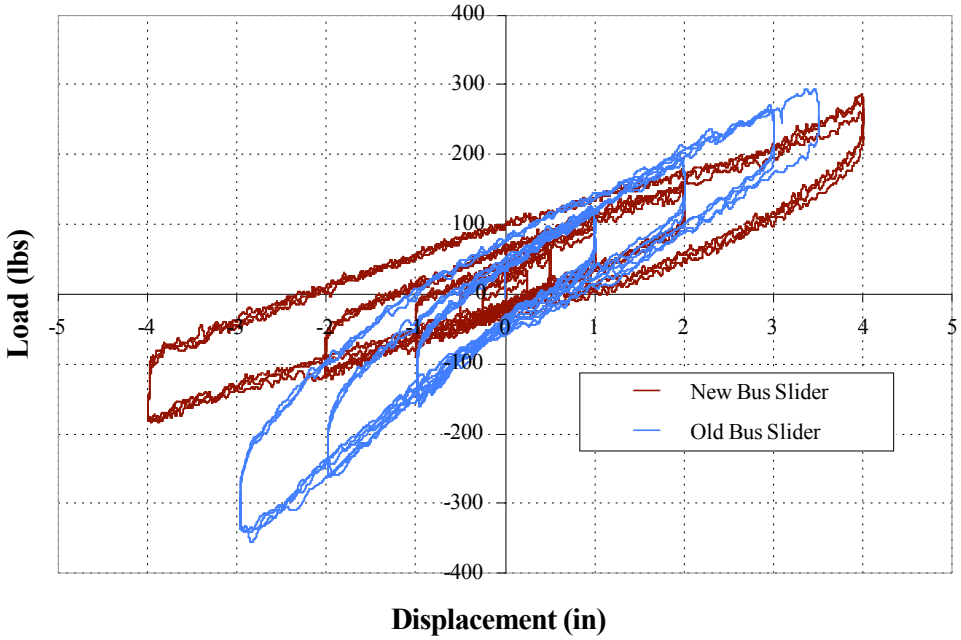

Figure 2.15 Bus Slider Connector Hysteresis Loops

The stiffness of the bus sliders was calculated in the same manner as the FSC specimens, wherein a trend line was applied to the data of each specimen. Table 2.3 summarizes the results and shows that the stiffness of the improved (new) bus slider is approximately 50% the stiffness of the original bus slider.

Table 2.3 Bus Slider Properties

Connector	Absolute Maximum Displacement (in)	Absolute Maximum Force (lbs)	Stiffness (lbs/in)
Original Bus Slider	3.50	354.9	89.1
Improved Bus Slider	4.00	284.1	43.6

2.8 EQUIVALENT VISCOUS DAMPING RATIOS

The energy dissipation capacity of the FSC specimens and bus slider, for different displacement amplitudes, can be characterized by an equivalent viscous damping ratio, ζ. This equivalent damping ratio corresponds, for a given displacement amplitude, to a purely viscous dashpot that will dissipate the same amount of energy per cycle as the real connectors. Based on the hysteresis loops for the specimens, the equivalent viscous damping ratio of a connector, ζ, at a given displacement amplitude, δ, is given by (Clough and Penzien, 1993):

$$\zeta = \frac{E_{D\delta}}{2\pi F_{\delta}\, \delta} \tag{2.2}$$

where $E_{D\delta}$ is the energy dissipated per cycle at a displacement amplitude δ, and F_{δ} is the force at the displacement amplitude δ.

Tables 2.4 and 2.5 present the equivalent viscous damping ratios for the three previously tested FSC specimens and both S-FSCs, respectively. Table 2.6 presents the equivalent damping ratios for the original and improved bus sliders. The values presented correspond to the mean values of the different cycles for a given displacement amplitude. Figures 2.16 and 2.17 compares graphically these same results.

For all FSC specimens, the equivalent damping ratios increase with displacement amplitude, indicating higher energy dissipation capacity at large inelastic displacements. One interesting aspect about this data is that the first (mis-shaped) S-FSC exhibits the highest damping values. This is believed to result from the increased contact between the straps, resulting in more energy dissipation through friction. The second S-FSC specimen, on the other hand, exhibits lower damping and is comparable to the damping values of FSC 30-2021 and FSC 30-2022. The FSC 30-2023 specimen exhibits the lowest damping for the complete range of displacement amplitudes (Filiatrault et al., 1999).

For the bus slider connectors, both specimens display similar damping. It is difficult to predict the behavior of the original bus slider at small amplitudes since the specimen was not cycled at these levels; however, the trend of damping between 1 in to 3 in is similar to the damping of the improved bus slider in this same region.

Table 2.4 Equivalent Viscous Damping Ratios for FSC Specimens

FSC 30-2021		FSC 30-2022		FSC 30-2023	
Amplitude (in)	Equiv. Damping Ratio (%)	Amplitude (in)	Equiv. Damping Ratio (%)	Amplitude (in)	Equiv. Damping Ratio (%)
1.0	2.84	1.0	2.00	2.3	4.52
1.3	4.75	1.3	3.00	3.0	5.56
2.6	13.1	2.6	10.1	6.0	17.6
3.9	18.0	3.9	20.8	6.0	23.0
5.2	20.1	5.2	29.9		
6.5	---	6.5	31.3		

Table 2.5 Equivalent Viscous Damping Ratios for S-FSC Specimens

First S-FSC		Second S-FSC	
Amplitude (in)	Equivalent Damping Ratio (%)	Amplitude (in)	Equivalent Damping Ratio (%)
0.25	3.31	0.25	0.15
0.5	1.57	0.5	1.08
1.0	4.99	1.0	1.63
2.0	14.57	2.0	4.22
4.0	24.66	4.0	---

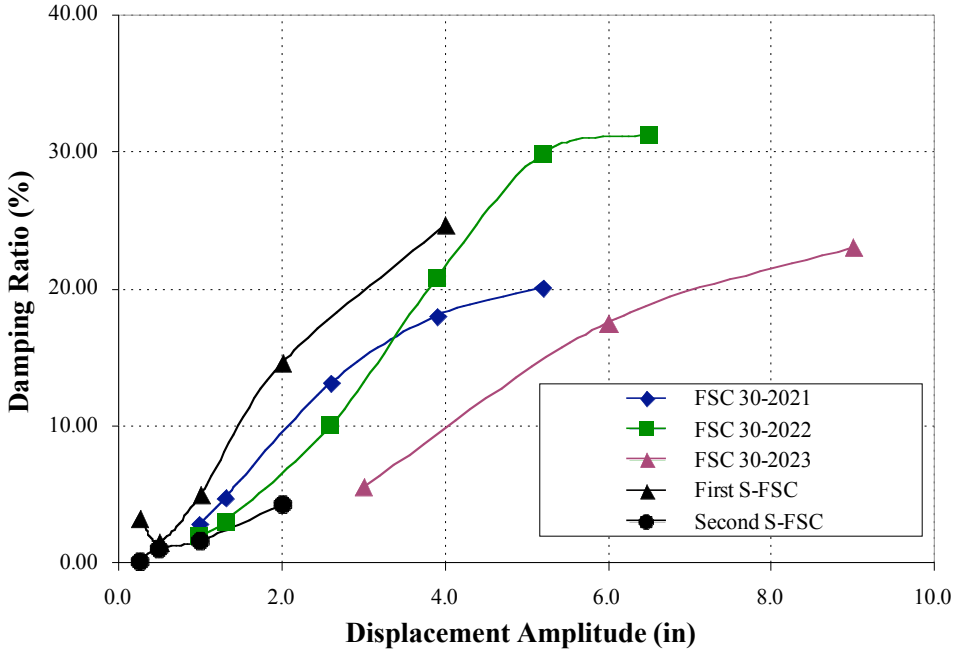

Figure 2.16 Comparison of Equivalent Viscous Damping Ratios for FSC Specimens

Table 2.6 Equivalent Viscous Damping Ratios for Bus Slider

Original Bus Slider		Improved Bus Slider	
Amplitude (in)	Equiv. Damping Ratio (%)	Amplitude (in)	Equiv. Damping Ratio (%)
1.0	19.13	0.25	45.82
2.0	17.46	0.5	27.52
3.0	15.63	1.0	20.64
--	--	2.0	15.06
--	--	4.0	12.37

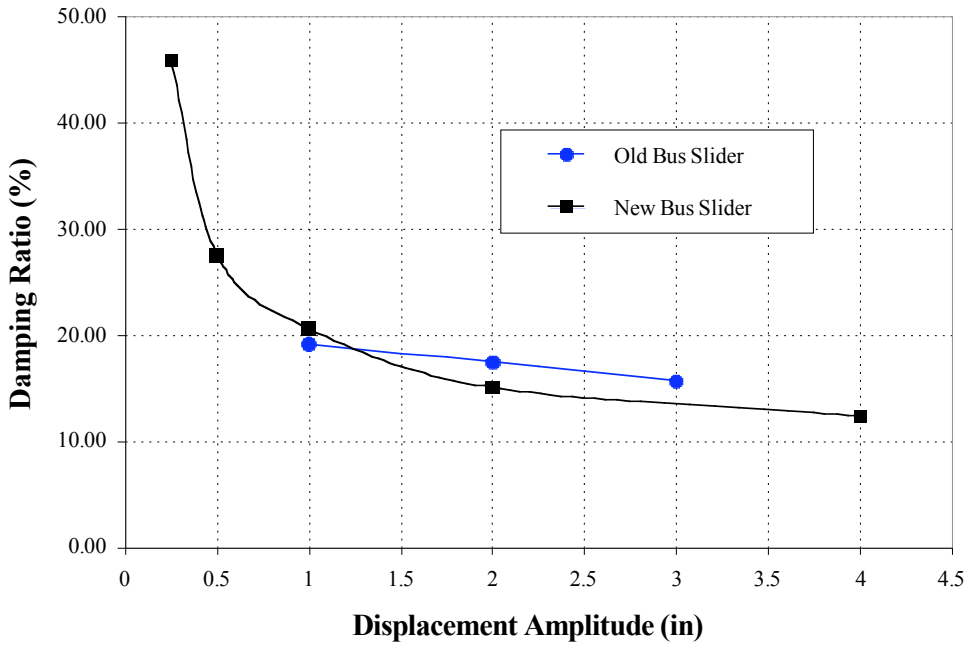

Figure 2.17 Comparison of Equivalent Viscous Damping Ratios for Bus Sliders

3. SHAKE TABLE TESTS OF PAIRS OF GENERIC SUBSTATION EQUIPMENT INTERCONNECTED WITH RIGID BUS ASSEMBLIES

3.1 INTRODUCTION

This chapter describes the shake table tests performed on five pairs of generic substation equipment connected with the three different rigid bus assemblies considered in this study. Simulated horizontal ground motions were applied in the longitudinal direction of the bus assemblies by the uniaxial earthquake simulation facility at UC-San Diego. The variables considered in the tests were:

- the dynamic characteristics of the generic equipment
- the types of rigid bus assemblies
- the simulated ground motions
- the intensities of the simulated ground motions

3.2 DESCRIPTION OF UC-SAN DIEGO UNIAXIAL EARTHQUAKE SIMULATION FACILITY

The uniaxial earthquake simulation system at UC-San Diego features a 4.8-ton shake table made of an all-welded steel construction, as shown in Figure 3.1. The shake table has plan dimensions of 10 ft x 16 ft with a specimen payload capacity of 40 tons. A 90-kip fatigue-rated actuator drives the system. The bearing system consists of eight 5-in Garlock DU cylinders sliding on two stationary shafts. The usable peak-to-peak stroke is 12 in. The flow rate of the hydraulic system allows a peak sinusoidal velocity of 40 in/s. The actuator can induce peak accelerations of 9.0 g for the bare

table and 1.0 g for the fully loaded table. The workable frequency range of the simulator spans from 0 to 50 Hz.

The control system of the shake table includes an advanced, second generation, digital controller incorporating a Three-Variable-Control (TVC), together with Adaptive Inverse Control (AIC), On-Line Iteration (OLI) techniques and Resonance Canceling Notch Filters. This advanced control system allows the reproduction of earthquake ground motions with high fidelity (Filiatrault et al., 1996, 2000).

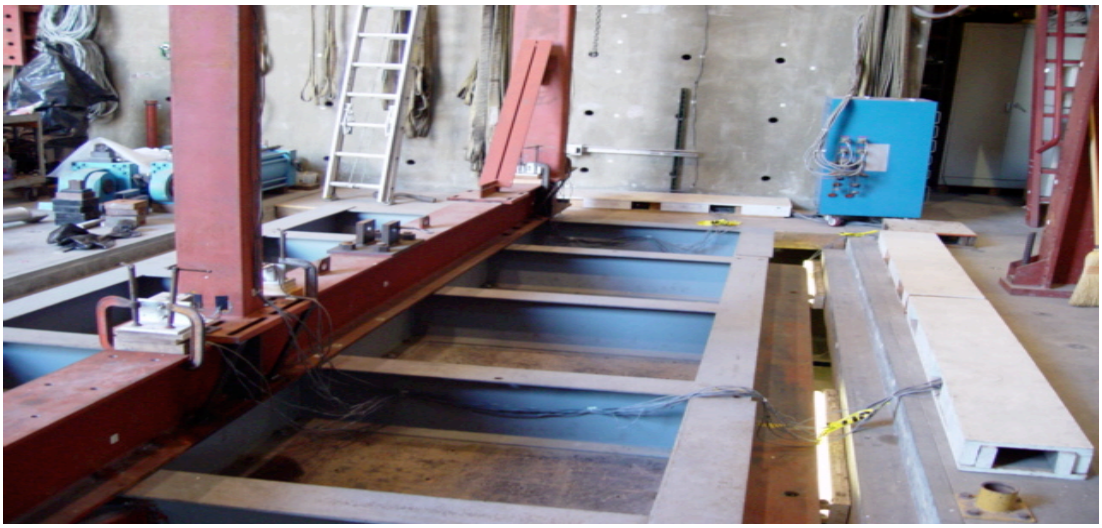

Figure 3.1 Shake Table of the UC-San Diego Uniaxial Earthquake Simulation System

3.3 DESCRIPTION OF GENERIC SUBSTATION EQUIPMENT

Five different pairs of generic substation equipment were considered for the shake table tests. Each pair of generic equipment was designed to be representative of the range of dynamic properties of actual interconnected substation electrical equipment (Filiatrault et al., 1999). Table 3.1 presents the target dynamic characteristics of the five pairs of generic equipment. It must be noted, that these tabulated target natural frequencies were not the resulting frequencies chosen for the Task 2C program in

1999. From Task 2C, these frequencies were targeted; however, the experimental frequencies were found to be slightly different from the target frequencies. Table 3.2 presents the resulting frequencies and the seismic weights of the equipment used in the Task 2C study. To remain consistent with the results, these resulting frequencies were used in this project.

Table 3.1 Target Dynamic Characteristics of Pairs of Generic Equipment

Pair	Equipment A			Equipment B		
	Equipment No.	Seismic Weight (lbs)	Natural Frequency (Hz)	Equipment No.	Seismic Weight (lbs)	Natural Frequency (Hz)
1	1	1000	1.5	3	250	5.0
2	1	1000	1.5	4	350	7.5
3	2	200	1.5	3	250	5.0
4	2	200	1.5	4	350	7.5
5	1	1000	1.5	5	350	12.0

Table 3.2 Dynamic Characteristics of Pairs of Generic Equipment Used in Task 2C (after Filiatrault et al. 1999)

Pair	Equipment A			Equipment B		
	Equipment No.	Seismic Weight (lbs)	Natural Frequency (Hz)	Equipment No.	Seismic Weight (lbs)	Natural Frequency (Hz)
1	1	557	1.99	3	197	4.10
2	1	557	1.99	4	363	5.47
3	2	92	1.88	3	197	4.10
4	2	92	1.88	4	363	5.47
5	1	557	1.99	5	68	12.23

From Table 3.2, five different generic equipment specimens are required to satisfy the test schedule. For each specimen, the seismic weight and natural frequency are fixed. Therefore, the design variables are the lateral stiffness of each specimen and the

appropriate strength to assure an elastic dynamic response. For simplicity, cantilevered columns anchored to a frame attached to the shake table surface represented the equipment items. Figure 3.2 illustrates the test set-up for the shake table tests. In order to mobilize sufficient strength for a given lateral stiffness, the height of all cantilevers was fixed at 14 ft. Table 3.3 presents the tubular steel sections used to fabricate each column. Appendix B presents the shop drawings used to fabricate the specimens.

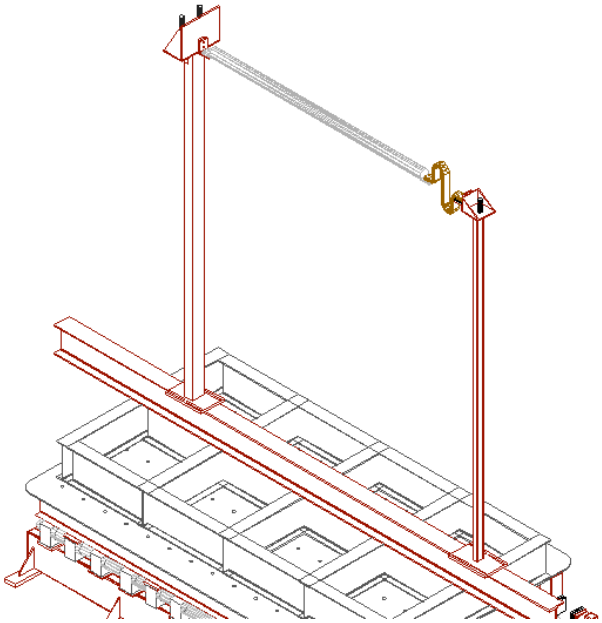

Figure 3.2 Test Set-Up for Shake Table Tests

Table 3.3 Tubular Steel Sections Used for Generic Equipment Specimens

Equipment	Seismic Weight (lbs)	Natural Frequency (Hz)	Tubular Section
1	557	1.99	7x5x3/16 in
2	92	1.88	3-1/2x2-1/2x1/4 in
3	197	4.18	8x6x3/16 in
4	363	5.47	12x8x5/16 in
5	68	12.15	12x8x5/16 in

Note that Equipment 5 is the same as Equipment 4, but incorporates a lateral bracing member (2 angles 3x3x3/8 back-to-back) to increase its target natural frequency to approximately 12 Hz. Figure 3.3 presents a photograph of Equipment 5.

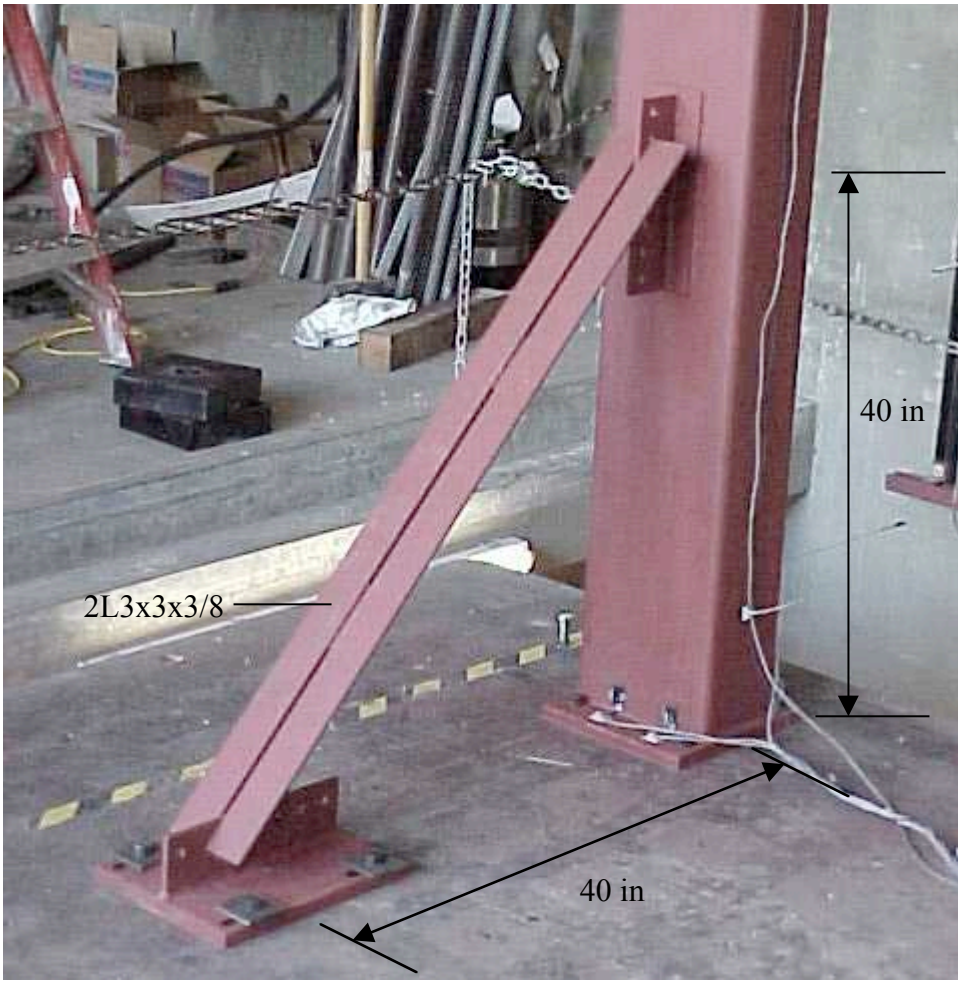

Figure 3.3 Equipment 5

In order to adjust the natural frequency of each equipment specimen, supplemental weights were added at the top of the columns, as illustrated in Figure 3.4. Table 3.4 indicates the final lumped weight added at the top of each specimen along with the total weight of each specimen.

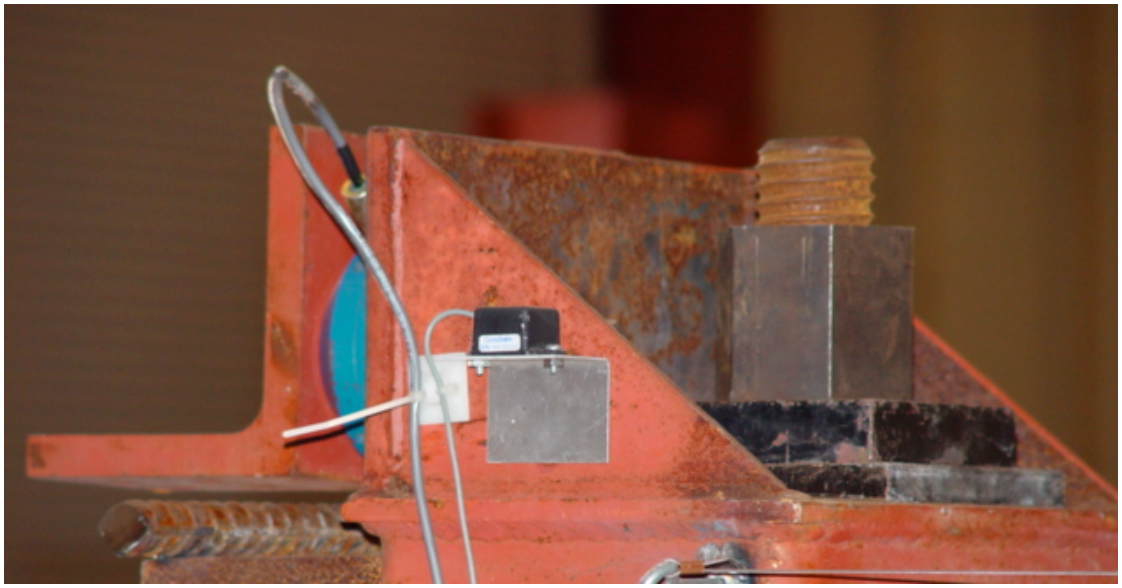

Figure 3.4 Supplemental Steel Weights at Top Generic Equipment Specimen

Table 3.4 Values of Lumped Weights at Top of Generic Equipment Specimens

Equipment	Target Seismic Weight (lbs)	Target Natural Frequency (Hz)	Lumped Top Weight (lbs)	Total Weight (lbs)
1	557	1.99	430	557
2	92	1.88	60	92
3	197	4.18	165	197
4	363	5.47	330	363
5	68	12.15	35	68

One concern that was apparent during testing of the equipment was the transverse rocking of the equipment at the base. During the tests, the equipment items were bolted down through the top flange of a W8x67 I-beam. It became apparent that due to the inertial effects of the equipment and the flexibility of the I-beam web, stiffeners would be needed at the base to achieve sufficient rigidity. Two types of stiffeners were used for this purpose. First, four 3 in x 3/8 in steel flats were welded at the four

corners of the equipment. The other ends were then welded to the bottom flange of the I-beam. Second, two 1/2 in thick steel plates were welded to the beam flanges and web. These plates were welded on each side of the beam, and attached directly beneath the center of the equipment. Figure 3.5 illustrates these stiffeners.

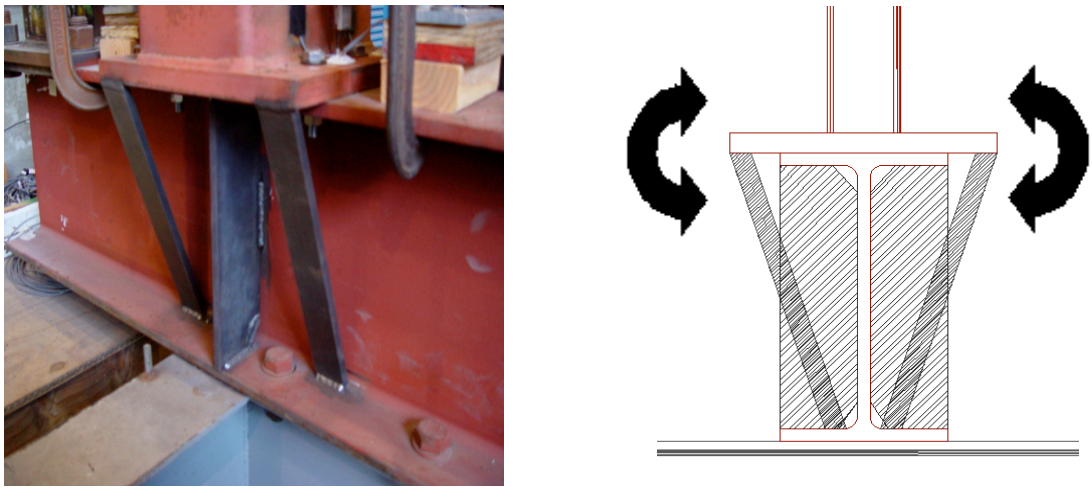

Figure 3.5 Base Stiffeners

3.4 INSTRUMENTATION

The instrumentation used during the shake table tests of the generic interconnected equipment included the following measurements:

- Absolute displacement, velocity and acceleration of the shake table
- Absolute displacement, velocity and acceleration at the top of each equipment
- Horizontal force at both ends of the conductor
- Axial strain at four locations in the S-FSC specimen

The velocity measurements were obtained directly with special string potentiometers calibrated to velocity.

3.5 EARTHQUAKE GROUND MOTIONS AND SHAKE TABLE FIDELITY

Two recorded components of near-field earthquake ground motions were used for the seismic tests of the shake table: Tabas (1978 Iran earthquake) and Newhall (1994 Northridge, California, earthquake). These two records are representative of earthquakes known to have a high potential for damaging structures and equipment. Figure 3.6 presents the acceleration time-histories for both full-scale records (full scale herein is referred as 100% span).

The Tabas record was modified using a non-stationary response-spectrum matching technique developed by Abrahamson (1997) to match the IEEE 693 target response spectrum for testing, and it was further high-pass filtered using a cut-off frequency of 1.5 Hz so as not to exceed the displacement limit of 6 in of the shake table.

Preliminary nonlinear dynamic time-history analyses were performed to estimate the response of the interconnected equipment. Based on the results of these preliminary analyses, different intensities were retained for each ground motion record. Table 3.5 presents these intensities for the two ground motions considered. Note that certain tests were not conducted at high intensity levels in order to prevent yielding of the generic equipment items.

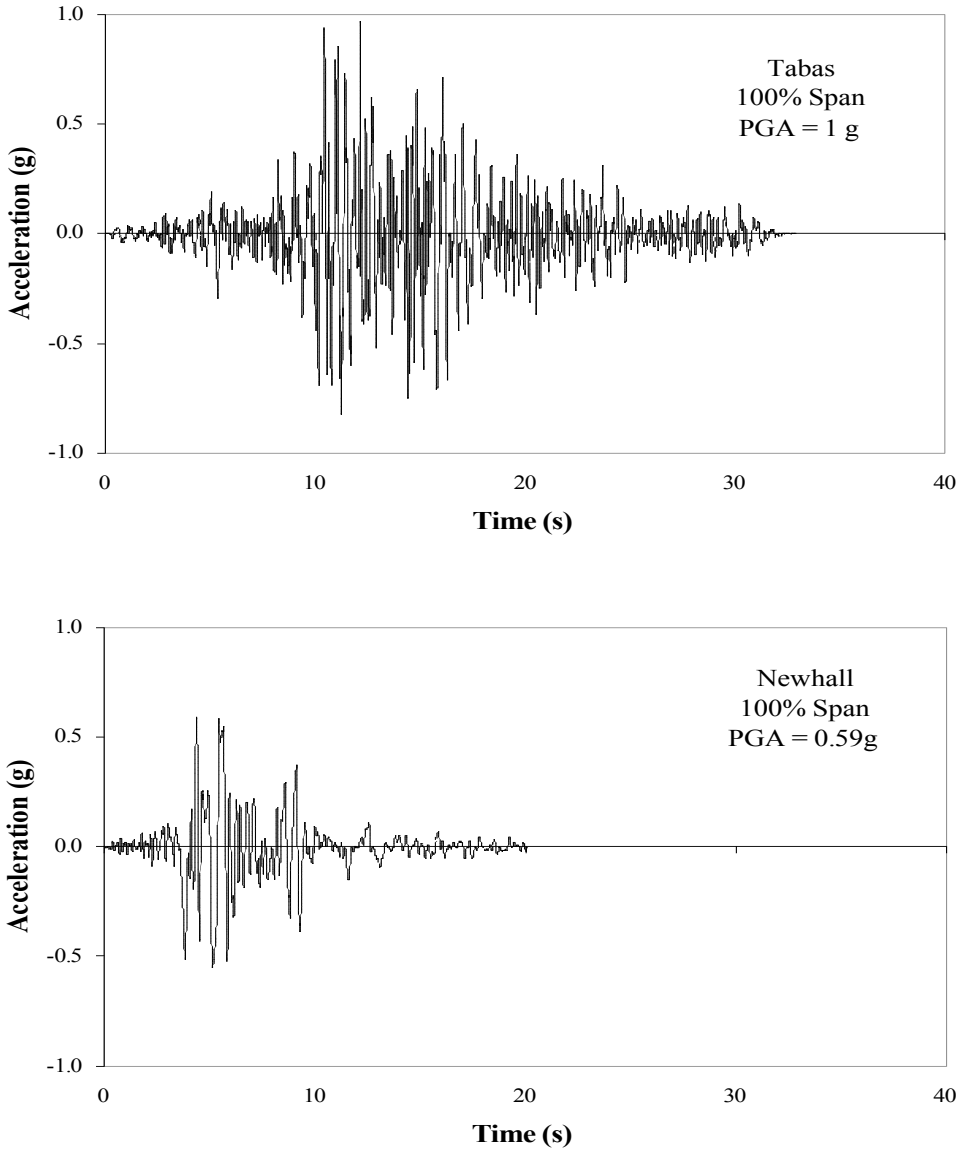

Figure 3.6 Acceleration Time-Histories of Earthquake Ground Motions

Table 3.5 Intensities of Earthquake Ground Motions Retained for Shake Table Tests

Record	Intensity 1 (% Span)	Intensity 2 (% Span)	Intensity 3 (% Span)
Tabas	25	50	100
Newhall	30	100	---

The performance of the shake table was optimized for each record and intensity using the On-Line Iteration (OLI) technique of the electronic controller. Figure 3.7 compares the absolute acceleration response spectra, at 2% damping, of the accelerograms of Figure 3.6 scaled at the different intensities listed in Table 3.5 (desired signals) with the response spectra of the acceleration time-histories recorded on the shake table (feedback signals). The feedback signals shown represent the mean values of three different tests on the shake table.

As discussed earlier, the original target natural frequencies of the generic equipment varied between 1.5 and 12 Hz. The mean differences (in %) between the desired and the feedback spectral values in the 1.5-12 Hz frequency range are also indicated in Figure 3.7. The maximum difference for all records is less than 6%. Based on this result, the performance of the shake table was considered adequate. For comparison purposes, each graph on Figure 3.7 also shows the IEEE 693 required response spectrum (at 2% damping) for high performance level amplified by a factor of two to account for the amplification of earthquake motion at the base of the generic equipment.

3.6 SHAKE TABLE TEST PROGRAM

Three different types of shake table tests were conducted on the pairs of generic equipment models interconnected by rigid bus assemblies:

1) Frequency Evaluation Tests
2) Damping Evaluation Tests
3) Seismic Tests

These tests are briefly described below.

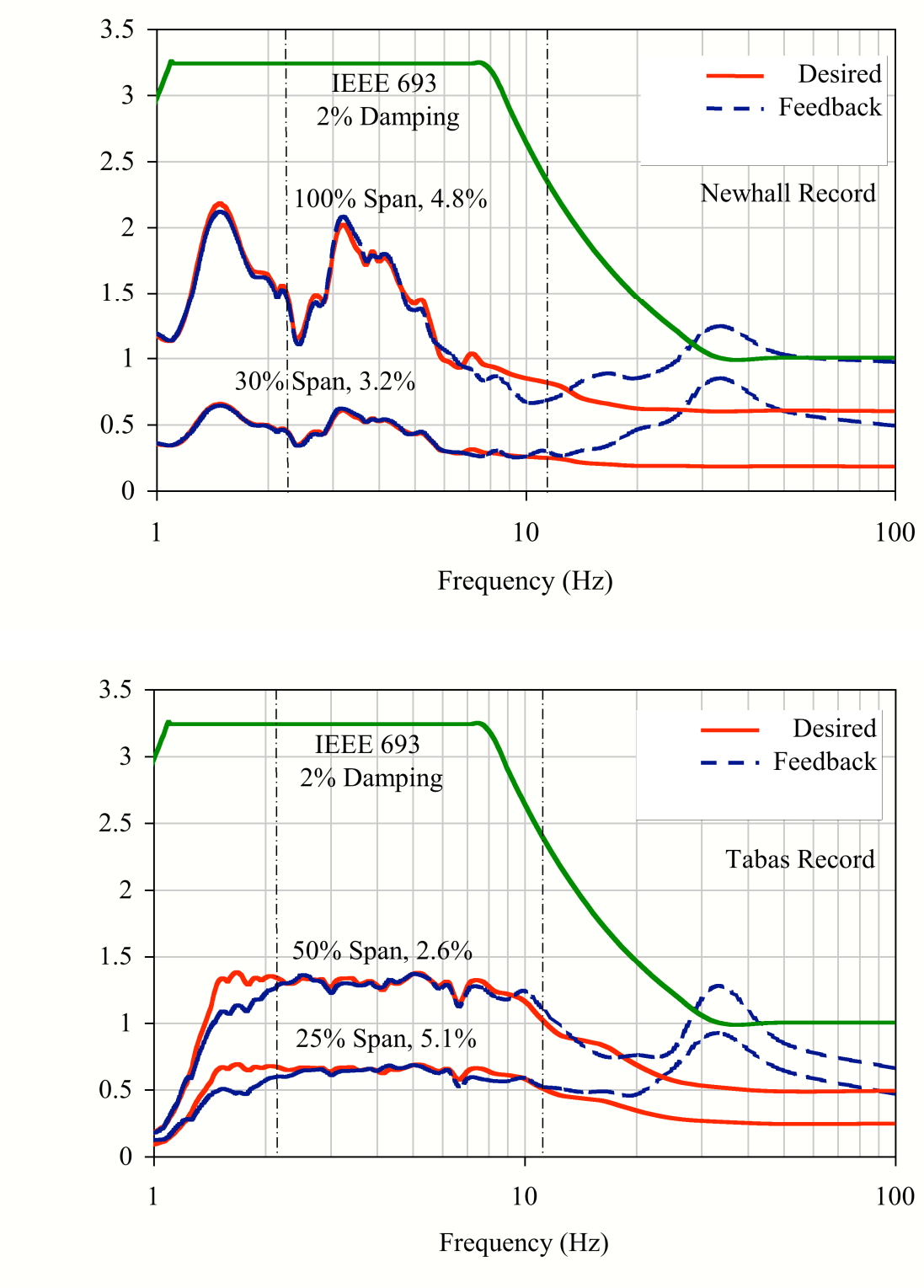

Figure 3.7 Absolute Acceleration Response Spectra, 5% Damping, Bare Shake Table

3.6.1 FREQUENCY EVALUATION TESTS

The purpose of the frequency evaluation tests was to identify the natural frequencies and mode shapes of the various pairs of interconnected generic equipment. For this purpose, a low-amplitude 0-40 Hz, clipped-band, and flat white noise base acceleration excited each configuration. A dedicated ambient vibration analysis software (Experimental Dynamic Investigations, 1993) was used to determine the natural frequencies from power spectral density plots of the absolute acceleration records at the top of each equipment. The natural frequencies were obtained from the amplitudes of the spectral peaks. For all frequency evaluation tests, the following protocol was followed:

- Nyquist frequency = 40 Hz
- Sampling rate = 80 Hz
- Number of points per sampling windows = 2048
- Duration of each sampling window = 25.6 s
- Frequency resolution = 0.0391 Hz
- Number of sampling windows = 8
- Total duration = 204.8 s

3.6.2 DAMPING EVALUATION TESTS

The purpose of the damping evaluation tests was to estimate the first equivalent modal viscous damping of each equipment configuration. In these tests, each pair of generic equipment was excited by a low-amplitude base sinusoidal input at its previously identified fundamental frequency. When a steady-state response was obtained, the input was suddenly stopped and the absolute accelerations at the top of

the equipment were recorded. The first modal damping ratio of the structural configuration was then established by the logarithmic decrement method (Clough and Penzien, 1993).

3.6.3 SEISMIC TESTS

In the seismic tests, the ground motions defined in Section 3.5 excited the pairs of interconnected equipment. All seismic data was acquired at a sampling rate of 200 Hz and low-pass filtered at 20 Hz.

3.7 RIGID BUS SPECIMENS

Three different rigid bus connector assemblies were tested with each of the five pairs of interconnected equipment defined in Table 3.1. These rigid bus assemblies were:

1) The bus assembly with the S-FSC specimen described in Section 2.2.1.
2) The bus assembly with the bus slider described in Section 2.2.2
3) The bus assembly SEFCOR connector developed by SDG&E described in Section 2.2.3

The first two rigid bus specimens were tested previously under quasi-static loading as described in Chapter 2. As also mentioned, the S-FSC specimen used for the shake table tests was the second specimen incorporating the correct initial geometry. The third rigid bus specimen was provided by SDG&E for the shake table tests only, and was not tested under quasi-static loading.

3.8 TEST SEQUENCE

Table 3.6 presents the test sequence that was adopted for the shake table tests. Included are the frequency and damping evaluation tests, as well as the seismic tests under the various earthquake ground motion records.

Table 3.6 Shake Table Test Sequence

Test RC-#	Pair No.	Connector	Test Description	Input Signal	Span (%)
1	2	None	Frequencies of Uncoupled Equipment	White Noise	---
2	2		Damping - A	Sinusoidal	---
3	2		Damping - B	Sinusoidal	---
4	2		Seismic	Newhall	30
5	2		Seismic	Newhall	100
6	2		Seismic	Tabas	25
7	2		Seismic	Tabas	50
8	2	Flexible Strap Connector	Frequencies of Coupled Equipment	White Noise	---
9	2		Damping - A	Sinusoidal	---
10	2		Damping - B	Sinusoidal	---
11	2		Seismic	Newhall	30
12	2		Seismic	Newhall	100
13	2		Seismic	Tabas	25
14	2		Seismic	Tabas	50
15	2	Bus Slider Connector	Frequencies of Coupled Equipment	White Noise	---
16	2		Damping - A	Sinusoidal	---
17	2		Damping - B	Sinusoidal	---
18	2		Seismic	Newhall	30
19	2		Seismic	Newhall	100
20	2		Seismic	Tabas	25
21	2		Seismic	Tabas	50
22	5	None	Frequencies of Uncoupled Equipment	White Noise	---
23	5		Damping - B	Sinusoidal	---
24	5		Seismic	Newhall	30
25	5		Seismic	Newhall	100
26	5		Seismic	Tabas	25
27	5		Seismic	Tabas	50

Table 3.6 Shake Table Test Sequence (continued)

Test RC-#	Pair No.	Connector	Test Description	Input Signal	Span (%)
28	5	Flexible Strap Connector	Frequencies of Coupled Equipment	White Noise	---
29	5		Damping - A	Sinusoidal	---
30	5		Damping - B	Sinusoidal	---
31	5		Seismic	Newhall	30
32	5		Seismic	Newhall	100
33	5		Seismic	Tabas	25
34	5		Seismic	Tabas	50
35	5	Bus Slider Connector	Frequencies of Coupled Equipment	White Noise	---
36	5		Damping - A	Sinusoidal	---
37	5		Damping - B	Sinusoidal	---
38	5		Seismic	Newhall	30
39	5		Seismic	Newhall	100
40	5		Seismic	Tabas	25
41	5		Seismic	Tabas	50
41B	5		Seismic	Tabas	100
42	1	None	Frequencies of Uncoupled Equipment	White Noise	---
43	1		Damping - B	Sinusoidal	---
44	1		Seismic	Newhall	30
45	1		Seismic	Newhall	100
46	1		Seismic	Tabas	25
47	1		Seismic	Tabas	50
48	1	Flexible Strap Connector	Frequencies of Coupled Equipment	White Noise	---
49	1		Damping - A	Sinusoidal	---
50	1		Damping - B	Sinusoidal	---
51	1		Seismic	Newhall	30
52	1		Seismic	Newhall	100
53	1		Seismic	Tabas	25
54	1		Seismic	Tabas	50
55	1	Bus Slider Connector	Frequencies of Coupled Equipment	White Noise	---
56	1		Damping - A	Sinusoidal	---
57	1		Damping - B	Sinusoidal	---

Table 3.6 Shake Table Test Sequence (continued)

Test RC-#	Pair No.	Connector	Test Description	Input Signal	Span (%)
58	1	Bus Slider Connector	Seismic	Newhall	30
59	1		Seismic	Newhall	100
60	1		Seismic	Tabas	25
61	1		Seismic	Tabas	50
62	3	None	Frequencies of Uncoupled Equipment	White Noise	---
63	3		Damping - A	Sinusoidal	---
64	3		Seismic	Newhall	30
65	3		Seismic	Newhall	100
66	3		Seismic	Tabas	25
67	3		Seismic	Tabas	50
68	3	Flexible Strap Connector	Frequencies of Coupled Equipment	White Noise	---
69	3		Damping - A	Sinusoidal	---
70	3		Damping - B	Sinusoidal	---
71	3		Seismic	Newhall	30
72	3		Seismic	Newhall	100
73	3		Seismic	Tabas	25
74	3		Seismic	Tabas	50
75	3	Bus Slider Connector	Frequencies of Coupled Equipment	White Noise	---
76	3		Damping - A	Sinusoidal	---
77	3		Damping - B	Sinusoidal	---
78	3		Seismic	Newhall	30
79	3		Seismic	Newhall	100
80	3		Seismic	Tabas	25
81	3		Seismic	Tabas	50
81B	3		Seismic	Tabas	100
82	4	Flexible Strap Connector	Frequencies of Coupled Equipment	White Noise	---
83	4		Damping - A	Sinusoidal	---
84	4		Damping - B	Sinusoidal	---

Table 3.6 Shake Table Test Sequence (continued)

Test RC-#	Pair No.	Connector	Test Description	Input Signal	Span (%)
85	4	Flexible Strap Connector	Seismic	Newhall	30
86	4		Seismic	Newhall	100
87	4		Seismic	Tabas	25
88	4		Seismic	Tabas	50
88B	4		Seismic	Tabas	100
89	4	Bus Slider Connector	Frequencies of Coupled Equipment	White Noise	---
90	4		Damping - A	Sinusoidal	---
91	4		Damping - B	Sinusoidal	---
92	4		Seismic	Newhall	30
93	4		Seismic	Newhall	100
94	4		Seismic	Tabas	25
95	4		Seismic	Tabas	50
95B	4		Seismic	Tabas	100
96	2	SEFCOR Connector	Frequencies of Coupled Equipment	White Noise	---
97	2		Damping - A	Sinusoidal	---
98	2		Damping - B	Sinusoidal	---
99	2		Seismic	Newhall	30
100	2		Seismic	Newhall	100
101	2		Seismic	Tabas	25
102	2		Seismic	Tabas	50
103	5	SEFCOR Connector	Frequencies of Coupled Equipment	White Noise	---
104	5		Damping - A	Sinusoidal	---
105	5		Damping - B	Sinusoidal	---
106	5		Seismic	Newhall	30
107	5		Seismic	Newhall	100
108	5		Seismic	Tabas	25
109	5		Seismic	Tabas	50

3.9 RESULTS OF FREQUENCY EVALUATION TESTS

The detailed results of all frequency evaluation tests conducted on all generic equipment combinations are presented in Appendix C. Included are power spectral

density, phase, and coherence plots obtained from the absolute acceleration records at the top of each equipment item.

Table 3.7 summarizes the results of the frequency evaluation tests on the stand-alone (unconnected) generic equipment specimens and compares them to the natural frequencies of the equipment used in task 2C shown Table 3.2. The fundamental frequencies of all equipment items agree very well with the frequencies measured in Task 2C.

Table 3.7 Measured Natural Frequencies of Generic Equipment Items

Equipment	Measured Natural Frequency (± 0.04 Hz)	Natural Frequency Measured in Task 2C (± 0.04 Hz)
	Mode 1	
1	1.99	1.99
2	1.88	1.88
3	4.10	4.18
4	5.47	5.47
5	12.15	12.23

Tables 3.8 to 3.10 summarize the results of the frequency evaluation tests on the five pairs of generic equipment specimens interconnected by the three different rigid bus assemblies.

For the cases of the coupled frequencies, the issue arose of whether to consider the resulting equipment frequencies as the isolated equipment frequencies or the coupled system frequencies. Figures 3.8 and 3.9 illustrate the mode shapes measured on the Equipment Pair 2 coupled by both the S-FSC and bus slider. The mode shapes

for the equipment coupled by the S-FSC show that this connector provided a very small system coupling effect, and therefore, the response of one equipment items influenced the other equipment item very little. The bus slider connector, however, did largely influence the system as can be seen by the mode shape values. Despite this large influence, the respective equipment frequencies were considered as the isolated equipment frequencies. It should also be noted that the phase angles of these mode shapes varied from 25 to 45 degrees.

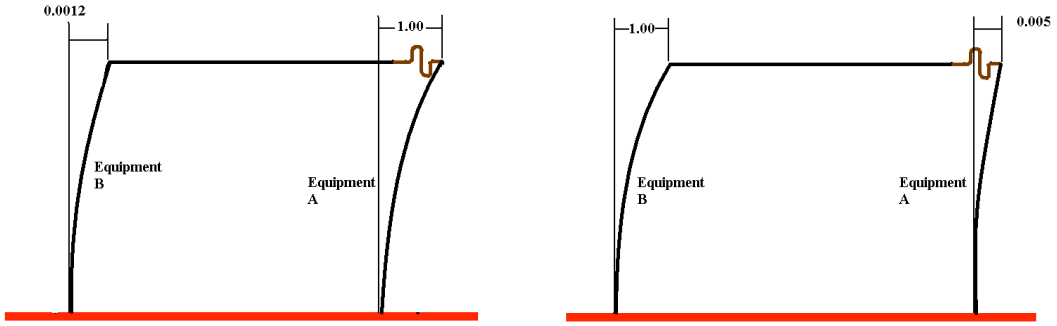

Mode 1 Mode 2

Figure 3.8 Mode Shapes of Equipment Pair 2 Interconnected by S-FSC Specimen

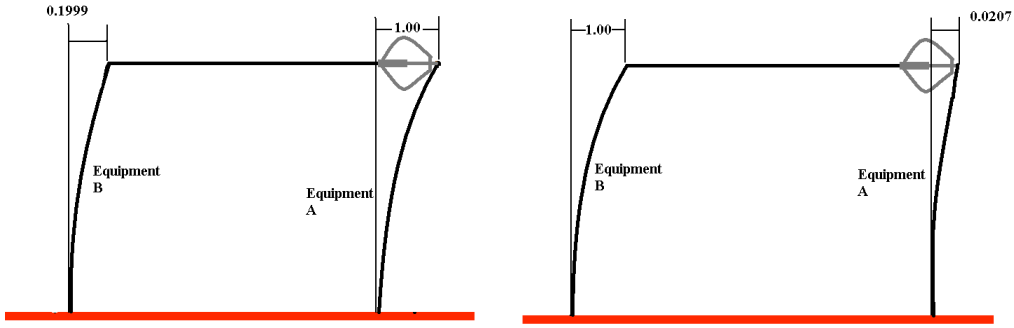

Mode 1 Mode 2

Figure 3.9 Mode Shapes of Equipment Pair 2 Interconnected by Bus Slider Connector

By examining the coupled/uncoupled frequency ratio, one can see exactly how much the connector is influencing the response of the generic equipment. The tendency is an increase of the lower frequency Equipment A, and a decrease of the

higher frequency Equipment B. In the case of the S-FSC and SEFCOR specimen, the coupling is not significant. The frequencies of the equipment items were well separated and associated with the vibration of a single equipment item as previously mentioned. The bus slider influenced the frequencies more substantially, however. The frequency ratios display a large deviation from 1.00

Table 3.8 Results of Frequency Evaluation Tests on Equipment Interconnected by S-FSC Specimen

Pair	Fundamental Frequency (± 0.04 Hz)			
	Equipment A	Coupled/Uncoupled Frequency Ratio	Equipment B	Coupled/Uncoupled Frequency Ratio
1	2.07	1.04	3.95	0.94
2	2.11	1.06	5.20	0.95
3	2.27	1.21	3.95	0.94
4	2.34	1.25	5.12	0.94
5	2.11	1.06	10.47	0.86

Table 3.9 Results of Frequency Evaluation Tests on Equipment Interconnected by Bus Slider

Pair	Fundamental Frequency (± 0.04 Hz)			
	Equipment A	Coupled/Uncoupled Frequency Ratio	Equipment B	Coupled/Uncoupled Frequency Ratio
1	2.42	1.22	2.42	0.58
2	2.58	1.29	5.27	0.96
3	3.09	1.65	3.24	0.78
4	2.93	1.56	5.16	0.94
5	2.07	1.04	10.27	0.85

Table 3.10 Results of Frequency Evaluation Tests on Equipment Interconnected by SEFCOR Connector

Pair	Fundamental Frequency (± 0.04 Hz)			
	Equipment A	Coupled/Uncoupled Frequency Ratio	Equipment B	Coupled/Uncoupled Frequency Ratio
2	1.99	1.00	5.20	0.95
5	1.99	1.00	10.66	0.88

The results shown in Tables 3.8 to 3.10 show that both sets of ratios for the S-FSC and the SEFCOR connector are comparable, indicating that the fundamental frequency of the equipment items are not affected significantly by the presence of the assemblies. In fact, the slight reduction seen here may be attributed to the added mass of the connector assemblies. The greater differences in frequency ratios between the S-FSC and the SEFCOR connector shows this added mass effect since the S-FSC assembly is much heavier than the SEFCOR specimen.

Of the three connectors tested, the ratios of the bus slider displayed the highest variability. Again, this is in part due to the added weight since the weight of this assembly is comparable to the S-FSC specimen assembly. The largest influence, however, is due to the resistance from the four cables on the specimen. In the process of performing these tests, this resistance was clear. When applying the random, white noise excitation to the equipment, it was evident that the bus slider was not sliding at the low excitations. A larger excitation amplitude was then applied to overcome this slip force. Even then, a large coupling force was observed. This coupling force resulted in the large variability in frequency ratios.

3.10 RESULTS OF DAMPING EVALUATION TESTS

The detailed results of all damping evaluation tests are presented in Appendix D. For each damping evaluation test, the logarithmic decrement method was applied to a succession of pairs of adjacent response cycles in order to obtain the variation of equivalent damping ratio with displacement amplitude. For this purpose, the displacement amplitude is defined as the mean amplitude of two adjacent response cycles.

Figure 3.10 presents the resulting variations of damping ratio with displacement amplitude for the five equipment items considered. For each equipment item, the results are presented for the uncoupled configuration and for all coupled configurations tested. The figures on the left show the results for all connectors. The figures on the right show a close-up of all the tests except the bus slider data. The data shows that the difference between the uncoupled and S-FSC specimen assembly is minimal. The damping provided by the S-FSC specimen is always just above or below the uncoupled case, which shows that very little damping is being added by the S-FSC specimen. The bus slider damping is clearly the most prominent. Due to the friction force from the connector, the response of equipment items tends to damp out quickly. The damping provided by the SEFCOR connector is more comparable to that of the S-FSC damping; however, it exhibited slightly higher damping than the S-FSC.

Another interesting result shown in the figure is the reduction of the damping ratio with displacement amplitude. This phenomenon occurs in about 50% of the tests and is contrary to the results observed for most structures where damping increases with

displacement amplitude. Further studies are required to better understand this phenomenon.

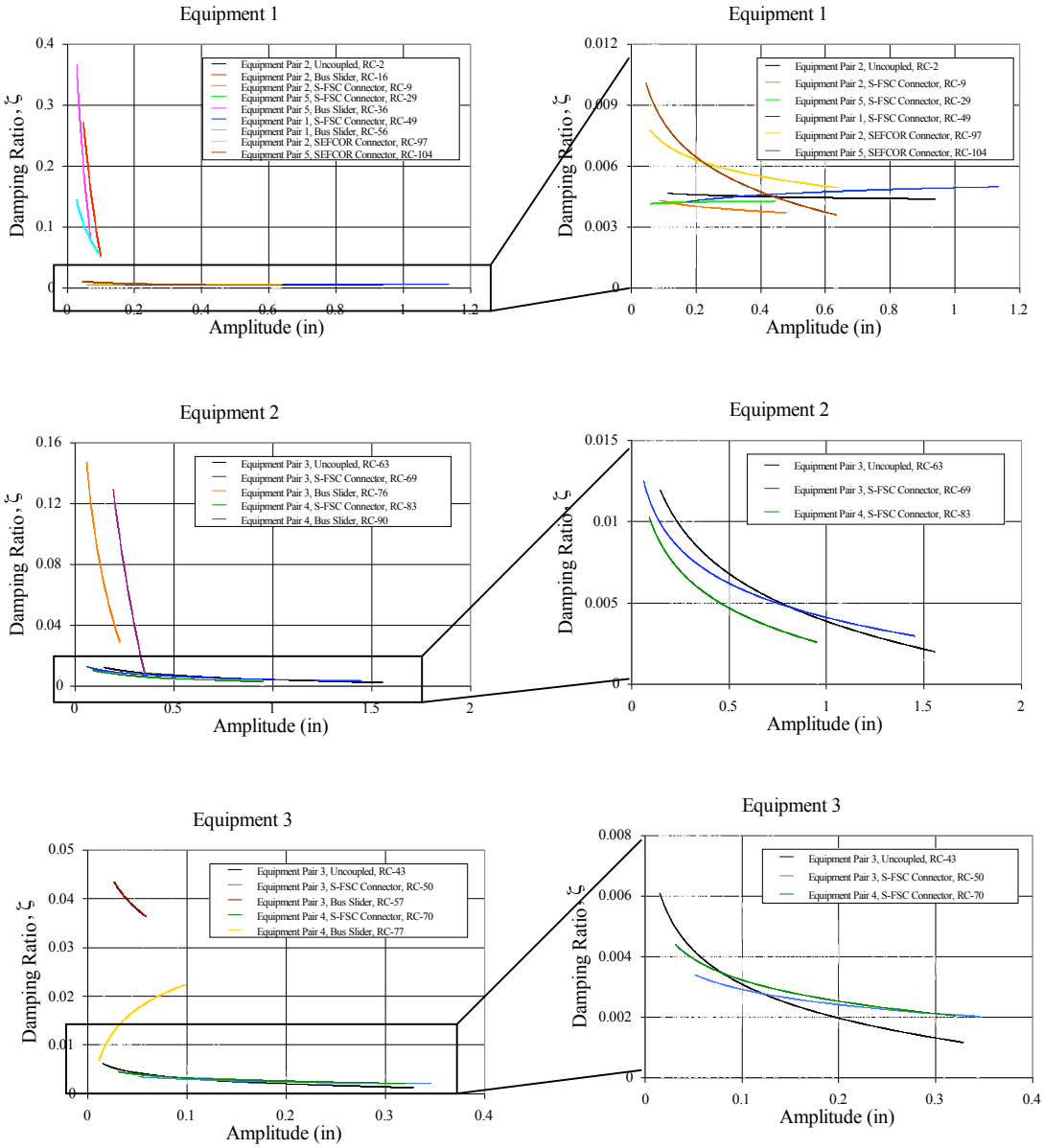

Figure 3.10 Variations of Equivalent Viscous Damping Ratio with Displacement Amplitude

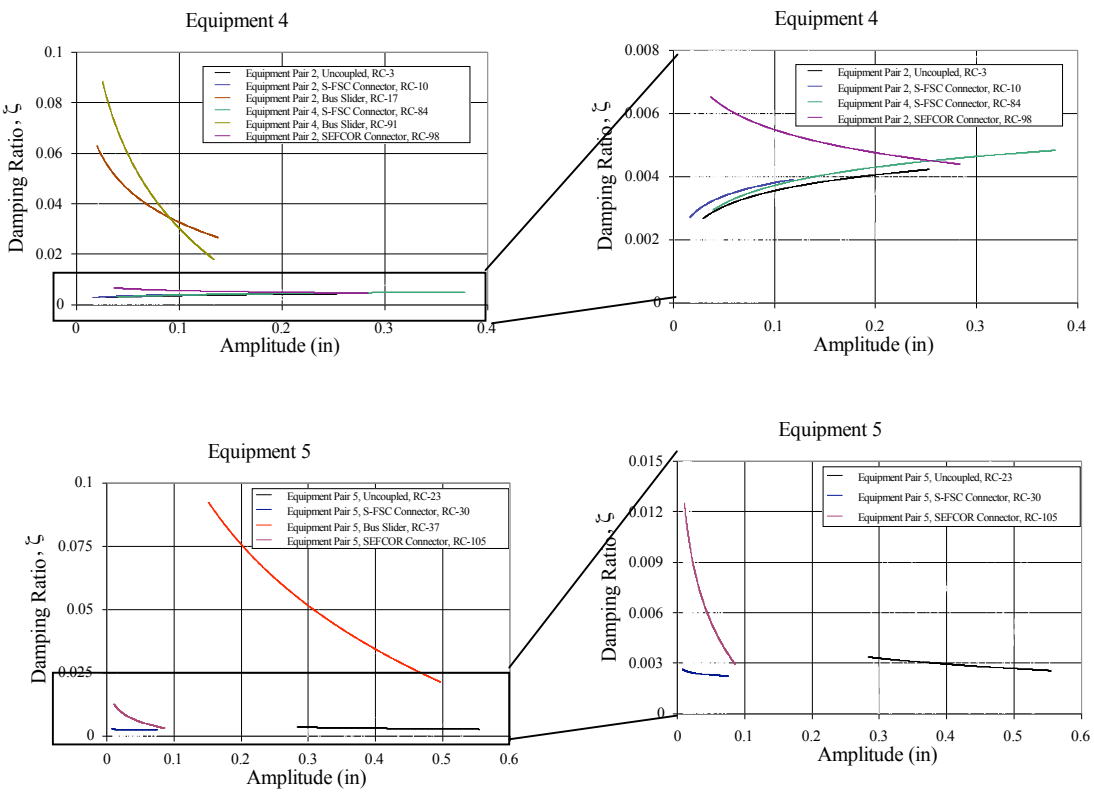

Figure 3.10 Variations of Equivalent Viscous Damping Ratio with Displacement Amplitude (continued)

3.11 RESULTS OF SEISMIC TESTS

The results of all seismic tests conducted on the five pairs of generic equipment specimens interconnected by the three different rigid bus assemblies are presented in Appendix E. Included for each seismic test are time-history plots of:

- Absolute acceleration of the shake table
- Relative horizontal displacement at the top of Equipment A
- Relative horizontal displacement at the top of Equipment B
- Absolute horizontal acceleration at the top of Equipment A
- Absolute horizontal acceleration at the top of Equipment B
- Relative displacement between Equipment A and Equipment B
- Horizontal force at the end of the conductor connected to Equipment A

- Horizontal force at the end of the conductor connected to Equipment B
- Force-displacement hysteresis loops at the connection of Equipment A
- Force-displacement hysteresis loops at the connection of Equipment B
- Strain values at instrumented locations on the S-FSC specimen

For the seismic tests involving the stand-alone (uncoupled) equipment, it was observed that some horizontal forces were measured by the load-cells at the top of each equipment item. These forces were developed because of the inertia effect of the load cells themselves and of the connecting elements. The seismic tests involving interconnected equipment were corrected for this inertia effect by first computing an equivalent load cell mass m_{lc} as:

$$m_{lc} = \frac{F_u}{a_u} \tag{3.1}$$

where F_u is the force measured by the load cell at the top of an equipment during an uncoupled seismic test and a_u is the horizontal acceleration measured at the top of an equipment during an uncoupled seismic test. Through this method, the load cell mass was found for every equipment pair and ground motion. For each pair, the typical load cell mass value was approximately 15 lbs, which is close to the actual weight of the load cell used.

The net horizontal force F_{nh} developed during a coupled seismic test was then computed by:

$$F_{nh} = F_c - m_{lc} a_c \tag{3.2}$$

where F_c is the force measured by the load cell at the top of an equipment during a coupled seismic test and a_c is the horizontal acceleration measured at the top of the

equipment under consideration. This net horizontal force is reported in Appendix E for each equipment item under consideration.

The results of the seismic tests showed that the S-FSC specimen remained elastic for all the tests with the Newhall earthquake at 30% span and Tabas at 25% span. However, for Newhall at 100% span and Tabas at 50% span and 100% span, the data from the strain gauges exceeded the yield strain of 1915 $\mu\varepsilon$. The highest yield strain resulted from test RC-88B where Equipment Pair 4 experienced the Tabas earthquake at 100% span. The maximum strain from the connector from this test was 3801 με, nearly twice the yield strain. Despite this yielding, due to the stiffness of the equipment items, the connector typically returned near its original position.

The bus slider specimen displayed overall good behavior except when being subjected to the Tabas record at 50% and 100% span. In most of these tests, the plunger was extended to the maximum possible stroke of 5 in. When this occurred, the stoppers at the end of the slider made contact with the tube and the specimen became rigid. Consequently, very high impact forces were transferred to equipment items. The maximum force that was transferred occurred in test RC-61, where a force of almost 2400 lbs was measured.

The SEFCOR connector behaved similarly to the S-FSC specimen. Low levels of forces were transmitted to the equipment while the original position was kept. Despite not undergoing high amplitude seismic tests like the other specimens, it is believed that due to the large loop of the cable, the specimen would not have become taut under these high amplitude tests.

The maximum experimental values recorded for all seismic tests are summarized in Tables 3.11 and 3.12. Included in these tables for each seismic test are the maximum relative displacement and maximum absolute acceleration at the top of both equipment specimens. The results for the stand-alone (uncoupled) tests are also included. Also presented in Tables 3.13 and 3.14 are the same results from the Task 2C project for the FSC 30-2022 connector and the original bus slider specimen (Filiatrault et al., 1999).

The effect of the various connectors on the dynamic response of the generic equipment specimens can be evaluated by defining a Displacement Amplitude Factor (DAF) and an Acceleration Amplification Factor (AAF) as (Der Kiereghian et al., 1999; Filiatrault et al., 1999; Filiatrault and Kremmidas, 2000):

$$\begin{aligned} DAF &= \frac{\text{Maximum Relative Displacement of Interconnected Equipment}}{\text{Maximum Relative Displacement of Stand Alone Equipment}} \\ AAF &= \frac{\text{Maximum Absolute Acceleration of Interconnected Equipment}}{\text{Maximum Absolute Acceleration of Stand Alone Equipment}} \end{aligned} \tag{3.3}$$

The DAF and AAF values computed at the top of Equipment A and Equipment B during the seismic tests are presented in Figures 3.11 and 3.12. The results are presented for each ground motion and intensity level for Equipment Pairs 2 and 5.

The presence of the rigid bus connectors can amplify or reduce the dynamic response of equipment components depending on their dynamic characteristics, the frequency content and intensity of the earthquake ground motion input. The results presented in the figures show several clear trends.

First for the majority of tests with the new bus slider, the DAF values were closer to the value of 1.0 than tests with the original specimen. In other words, the response of the equipment interconnected by the new specimen behaved more like uncoupled specimens. The SEFCOR connector DAF values showed very little variance from 1.0. Due to the high flexibility of the specimen, the equipment items acted nearly identical to the stand-alone equipment.

Another trend that was observed was the lower AAF values attained for the improved connectors. In most cases, the AAF values for the S-FSC specimen were reduced when compared to the tests with the FSC 30-2022 connector. The bus slider results show that, in general, the improved slider caused similar AAF values as that of the original slider. Finally, the SEFCOR connector again exhibited the same behavior as the stand-alone situations with the AAF values being close to 1.0.

Table 3.11Peak Relative Displacements from Seismic Tests

Pair	Ground Motion Span (%)	Peak Relative Displacement Equipment A (in)			
		S-FSC	Bus Slider	SEFCOR	Stand Alone
1	Newhall 30%	1.92	1.12	--	2.25
	Tabas 25%	2.49	1.90	--	2.90
	Tabas 50%	4.94	3.69	--	4.64
2	Newhall 30%	1.65	1.05	2.18	2.26
	Tabas 25%	2.38	1.73	2.81	3.01
	Tabas 50%	4.56	3.60	4.70	4.60
3	Newhall 30%	1.99	0.84	--	1.85
	Tabas 25%	2.26	1.47	--	4.72
	Tabas 50%	4.07	2.94	--	9.58
4	Newhall 30%	1.31	0.72	--	1.85
	Tabas 25%	1.93	1.22	--	4.72
	Tabas 50%	3.58	2.55	--	9.58
5	Newhall 30%	1.58	0.98	2.19	2.25
	Tabas 25%	2.28	1.66	2.85	2.97
	Tabas 50%	4.39	3.46	4.66	4.67

Pair	Ground Motion Span (%)	Peak Relative Displacement Equipment B (in)			
		S-FSC	Bus Slider	SEFCOR	Stand Alone
1	Newhall 30%	0.93	0.51	--	0.48
	Tabas 25%	0.83	0.68	--	1.14
	Tabas 50%	1.66	1.81	--	2.28
2	Newhall 30%	0.24	0.19	0.25	0.25
	Tabas 25%	0.43	0.34	0.48	0.48
	Tabas 50%	0.73	0.70	0.79	0.71
3	Newhall 30%	0.80	0.36	--	0.47
	Tabas 25%	0.70	0.49	--	1.12
	Tabas 50%	1.39	1.09	--	2.26
4	Newhall 30%	0.27	0.23	--	0.25
	Tabas 25%	0.47	0.41	--	0.48
	Tabas 50%	0.77	0.80	--	0.71
5	Newhall 30%	0.08	0.10	0.08	0.07
	Tabas 25%	0.19	0.12	0.11	0.16

	Tabas 50%	0.31	0.24	0.27	0.24

Table 3.12 Peak Absolute Accelerations from Seismic Tests

Pair	Ground Motion Span (%)	Peak Absolute Acceleration Equipment A (g)			
		S-FSC	Bus Slider	SEFCOR	Stand Alone
1	Newhall 30%	0.89	0.60	--	1.00
	Tabas 25%	1.11	0.94	--	1.27
	Tabas 50%	2.22	3.24	--	1.92
2	Newhall 30%	0.82	0.58	0.93	1.02
	Tabas 25%	1.10	0.89	1.22	1.26
	Tabas 50%	1.95	2.05	1.91	1.92
3	Newhall 30%	1.18	0.74	--	0.79
	Tabas 25%	1.37	1.05	--	1.99
	Tabas 50%	2.57	2.22	--	4.12
4	Newhall 30%	0.84	0.62	--	0.79
	Tabas 25%	1.18	0.94	--	1.99
	Tabas 50%	2.28	1.77	--	4.12
5	Newhall 30%	0.81	0.53	0.95	0.96
	Tabas 25%	1.10	0.83	1.19	1.22
	Tabas 50%	1.91	1.97	1.93	1.89

Pair	Ground Motion Span (%)	Peak Absolute Acceleration Equipment B (g)			
		S-FSC	Bus Slider	SEFCOR	Stand Alone
1	Newhall 30%	1.33	0.64	--	0.87
	Tabas 25%	1.20	0.89	--	2.03
	Tabas 50%	2.40	3.27	--	4.04
2	Newhall 30%	0.65	0.59	0.78	0.84
	Tabas 25%	1.06	1.15	1.42	1.79
	Tabas 50%	2.38	2.23	3.07	2.85
3	Newhall 30%	1.22	0.53	--	0.90
	Tabas 25%	1.94	0.66	--	2.04
	Tabas 50%	2.00	1.50	--	3.99
4	Newhall 30%	0.74	0.65	--	0.84
	Tabas 25%	1.25	1.05	--	1.79
	Tabas 50%	1.93	2.22	--	2.85
	Newhall 30%	0.48	0.58	0.75	0.73

5	Tabas 25%	1.77	1.06	1.29	2.13
	Tabas 50%	2.92	2.47	2.86	3.06

Table 3.13 Peak Relative Displacements from Task 2C Seismic Tests

Pair	Ground Motion Span (%)	Peak Relative Displacement Equipment A (in)		
		FSC 30-2022	Old Bus Slider	Stand Alone
1	Newhall 30%	0.98	--	1.50
	Tabas 25%	1.69	--	2.06
	Tabas 50%	--	3.04	4.94
2	Newhall 30%	1.40	0.63	1.50
	Tabas 25%	1.56	1.00	2.06
	Tabas 50%	3.09	2.91	4.94
3	Newhall 30%	1.03	--	1.73
	Tabas 25%	1.68	--	3.04
	Tabas 50%	3.61	2.04	7.82
4	Newhall 30%	1.05	--	1.77
	Tabas 25%	0.92	--	2.94
	Tabas 50%	1.97	1.25	7.75
5	Newhall 30%	0.71	0.66	1.91
	Tabas 25%	1.05	0.81	3.23
	Tabas 50%	1.93	2.42	4.42

Pair	Ground Motion- Span (%)	Peak Relative Displacement Equipment B (in)		
		FSC 30-2022	Old Bus Slider	Stand Alone
1	Newhall 30%	0.70	--	0.63
	Tabas 25%	1.17	--	1.13
	Tabas 50%	--	1.15	2.00
2	Newhall 30%	0.67	0.29	0.40
	Tabas 25%	0.71	0.29	0.46
	Tabas 50%	1.27	0.61	0.98
3	Newhall 30%	0.79	--	0.63
	Tabas 25%	1.33	--	1.13
	Tabas 50%	2.72	1.09	2.00
4	Newhall 30%	0.55	--	0.36
	Tabas 25%	0.47	--	0.49
	Tabas 50%	0.95	0.45	0.96
	Newhall 30%	0.20	0.17	0.18

5	Tabas 25%	0.25	0.28	0.20
	Tabas 50%	0.36	0.31	0.34

Table 3.14 Peak Absolute Accelerations from Task 2C Seismic Tests

Pair	Ground Motion Span (%)	Peak Absolute Acceleration Equipment A (g)		
		FSC 30-2022	Old Bus Slider	Stand Alone
1	Newhall 30%	0.55	--	0.59
	Tabas 25%	1.01	--	0.81
	Tabas 50%	--	1.51	1.90
2	Newhall 30%	0.96	0.40	0.59
	Tabas 25%	1.07	0.56	0.81
	Tabas 50%	2.08	1.49	1.90
3	Newhall 30%	0.96	--	0.87
	Tabas 25%	2.00	--	1.17
	Tabas 50%	3.92	2.19	3.04
4	Newhall 30%	1.60	--	0.70
	Tabas 25%	1.54	--	1.11
	Tabas 50%	3.52	1.73	2.84
5	Newhall 30%	0.65	0.41	0.79
	Tabas 25%	1.02	0.47	0.73
	Tabas 50%	1.75	1.34	1.73

Pair	Ground Motion Span (%)	Peak Absolute Acceleration Equipment B (g)		
		FSC 30-2022	Old Bus Slider	Stand Alone
1	Newhall 30%	0.76	--	1.14
	Tabas 25%	1.13	--	1.97
	Tabas 50%	--	1.45	3.54
2	Newhall 30%	0.61	0.47	0.80
	Tabas 25%	0.85	0.53	1.19
	Tabas 50%	1.69	1.28	2.32
3	Newhall 30%	0.78	--	1.14
	Tabas 25%	1.28	--	1.97
	Tabas 50%	2.76	1.44	3.54
4	Newhall 30%	0.80	--	0.93
	Tabas 25%	0.75	--	1.20
	Tabas 50%	1.73	1.08	2.36
5	Newhall 30%	0.61	0.44	0.49
	Tabas 25%	0.98	0.60	1.71

	Tabas 50%	1.75	1.38	3.13

Equipment Pair 2

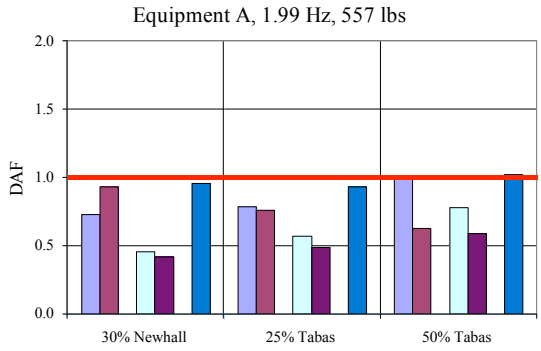

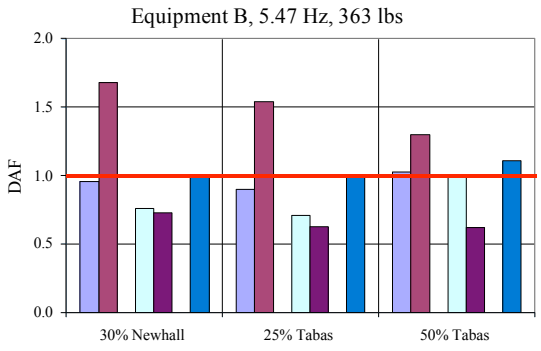

Equipment Pair 5

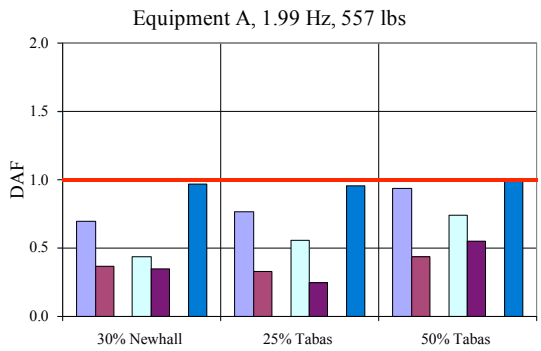

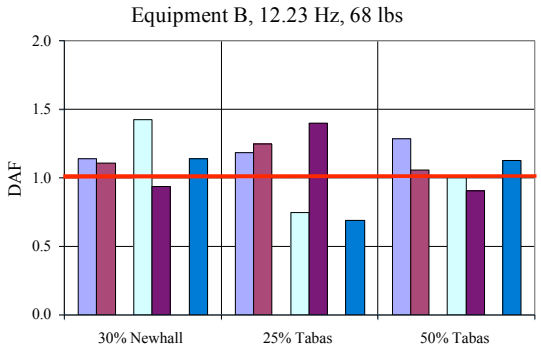

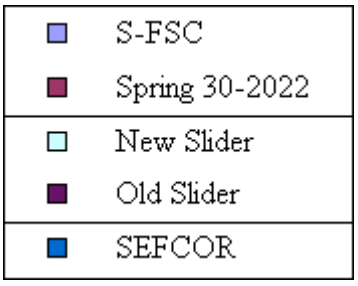

Figure 3.11 Displacement Amplification Factor (DAF) for Equipment Pairs 2 and 5

Equipment Pair 2

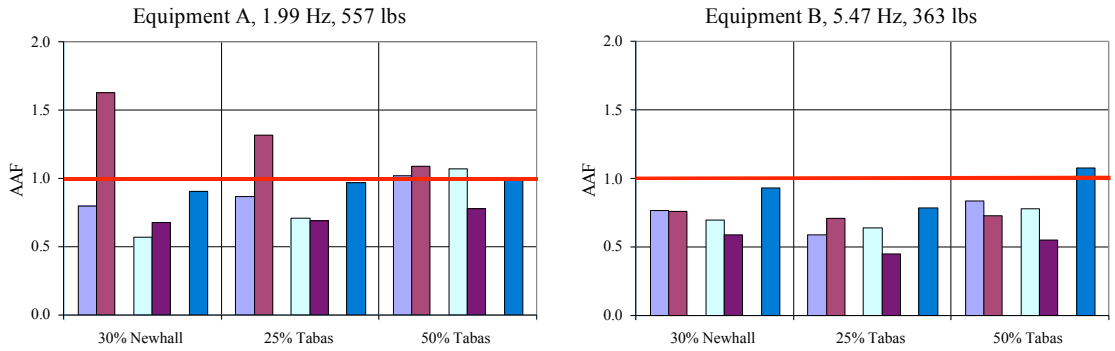

Equipment Pair 5

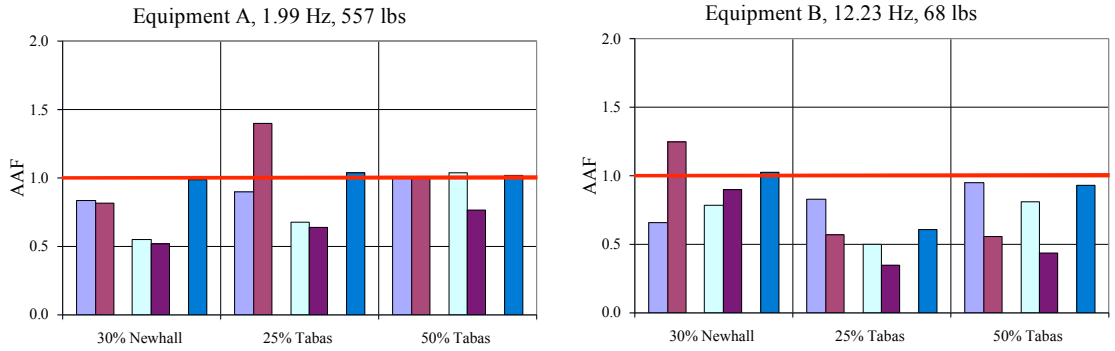

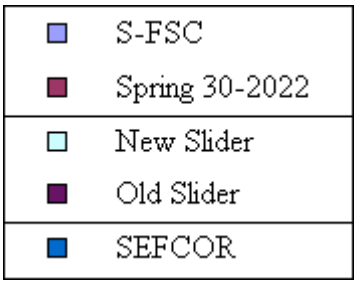

Figure 3.12 Acceleration Amplification Factor (AAF) for Equipment Pairs 2 and 5

The maximum horizontal forces in the conductors at the top of each of the interconnected equipment items recorded for all seismic tests are presented in Tables 3.15 and 3.16 for the current and the Task 2C sets of tests, respectively.

Table 3.15 Maximum Horizontal Forces in Connectors from Seismic Tests

Pair	Ground Motion Span (%)	Maximum Connector Force (lbs)		
		S-FSC	Bus Slider	SEFCOR
1	Newhall 30%	111	92	--
	Tabas 25%	123	110	--
	Tabas 50%	208	2393	--
2	Newhall 30%	89	97	46
	Tabas 25%	129	143	82
	Tabas 50%	204	283	161
3	Newhall 30%	97	64	--
	Tabas 25%	110	93	--
	Tabas 50%	172	185	--
4	Newhall 30%	81	63	--
	Tabas 25%	133	101	--
	Tabas 50%	185	184	--
5	Newhall 30%	82	94	40
	Tabas 25%	153	143	75
	Tabas 50%	265	242	169

Table 3.16 Maximum Horizontal Forces in Connectors from Task 2C Seismic Tests

Pair	Ground Motion Span (%)	Maximum Connector Force (lbs)	
		FSC 30-2022	Old Bus Slider
1	Newhall 30%	218	--
	Tabas 25%	293	--
	Tabas 50%	--	301
2	Newhall 30%	313	120
	Tabas 25%	373	137
	Tabas 50%	652	284
3	Newhall 30%	47	--
	Tabas 25%	110	--
	Tabas 50%	205	123
4	Newhall 30%	94	--
	Tabas 25%	93	--
	Tabas 50%	217	97
5	Newhall 30%	273	207
	Tabas 25%	478	168
	Tabas 50%	748	323

The comparison of maximum horizontal forces in the conductors developed at the top of the equipment during the seismic tests is presented in Figure 3.13. Again, the results are presented for Equipment Pairs 2 and 5 and for each ground motion, intensity level, and conductor type.

In all cases but one, the forces generated on the equipment by the improved connectors were reduced. For the S-FSC specimen, this reduction was very pronounced. Due to the higher flexibility of the new specimen, some of these tests showed a reduction of about one-third the forces from the Task 2C tests. Note, however, that the design of the new bus slider can lead to large impact forces when the bus is in tension, as opposed to the old bus slider. This phenomenon can be observed in Tables 3.15 and 3.16 for equipment pair 1 under the Tabas 50% ground motion.

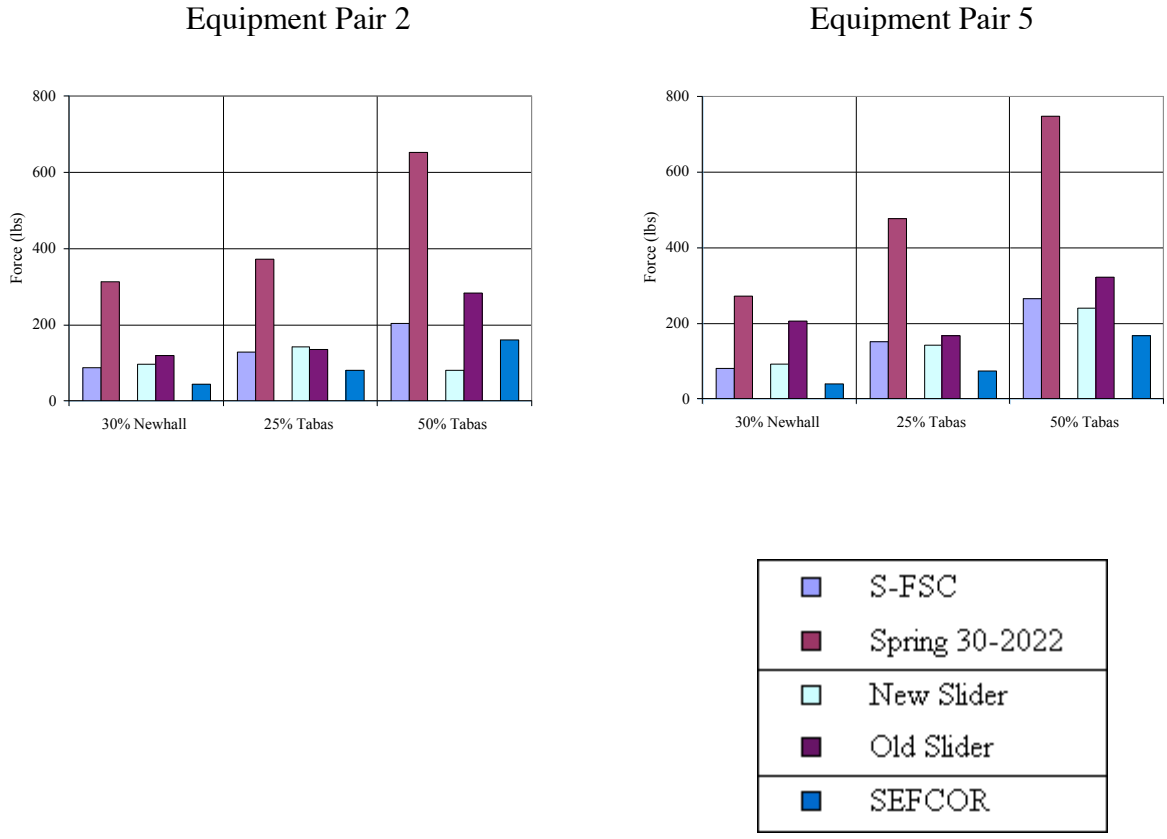

Figure 3.13 Maximum Horizontal Forces in Connectors for Equipment Pairs 2 and 5

Overall, the bus slider comparison showed the same trend as the S-FSC specimen. The forces generally were reduced from the Task 2C tests, but only slightly. In some cases, such as the tests involving Equipment Pairs 3 and 4, the forces from the improved (new) bus slider were higher. In these equipment pairs, the Equipment A specimen was Equipment 2, the most flexible of all the equipment items at 1.88 Hz. Consequently, the system should experience a large relative displacement between the equipment. This may have been the reason for the large forces produced with the new

bus slider. It must be noted that only the Tabas record at 50% span can be compared since the Task 2C program completed this test only for the bus slider. Table 3.17 summarizes the maximum relative displacements for the Tabas at 50% span test with the two equipment pairs. The comparison shows that the equipment with the original (old) bus slider experienced smaller relative displacements with small forces exerted on the equipment. Alternatively, the equipment with the improved (new) bus slider experienced much higher displacements and, consequently, the forces on the equipment were higher.

Table 3.17 Maximum Equipment Relative Displacement for Tabas 50%

	Maximum Relative Displacement (in)	
	Equipment Pair 3	Equipment Pair 4
Old Bus Slider	1.18	0.98
New Bus Slider	2.72	2.75

The forces exerted by the SEFCOR connector were relatively low. Due to the high flexibility, the resulting forces on the equipment were generally lower than the forces from the other specimens.

4. NUMERICAL MODELING

4.1 INTRODUCTION

In an effort to predict the experimental results obtained in this study, simplified numerical models were developed. The main purpose of the study was to assess the prediction capability of numerical models that could be developed by practicing engineers using available commercial computer software. For this purpose, the computer program RUAUMOKO (Carr 2000) was considered.

The program RUAUMOKO is designed to produce a piece-wise time-history response of a non-linear general two-dimensional framed structure to ground acceleration or time varying force excitation. The program was used to simulate both, the quasi-static tests and the shake table tests conducted on the improved SFSC and bus slider. The simulation of the quasi-static tests were based on cyclic push-over analyses using material properties and geometry of the connectors. The force-displacement hysteresis loops obtained in the quasi-static tests were compared against the numerical predictions. The simulation of the shake table tests were based on equivalent nonlinear connector elements incorporating the hysteretic behavior predicted by the numerical modeling of the quasi-static tests. Several displacement and acceleration time histories were obtained from these seismic analyses and compared with the experimental results.

4.2 MODELING OF QUASI-STATIC TESTS

4.2.1 MODEL DESCRIPTION

To model the quasi-static test conducted on the S-FSC specimen, 130 nonlinear straight beam elements were used to approximate the geometry of the connector. In the curved regions, many elements were implemented to create smooth representations of the curves and to achieve accurate results for the points of maximum bending. In the straight regions, fewer elements were used. Figure 4.1 presents the RUAUMOKO beam element mesh for the connector. The figure shows an overall accurate shape; however, the graphic output of the program does not capture the complete curved regions due to the dense number of elements used in this region.

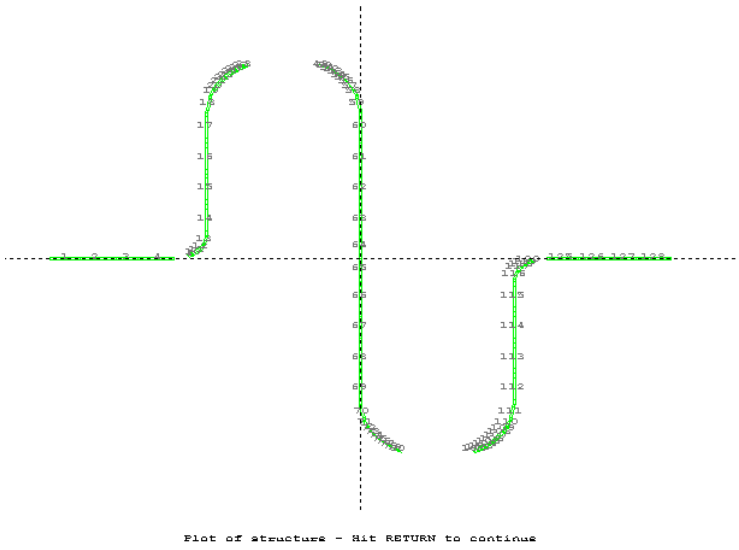

Figure 4.1 RUAUMOKO Beam Element Mesh of S-FSC

The properties of the beam elements used in the numerical model are shown in Table 4.1. The beam elements used in the model exhibited bi-linear moment-curvature hysteretic behavior. The elastic flexural stiffness values were obtained from the

original coupon tests of the copper alloy material. The cross-sectional properties of the beam elements were calculated from the geometry of the flexible straps. It was assumed that the beam elements could deform elastically in their axial directions. The bi-linear factor, defined as the ratio of post-yield flexural stiffness to the elastic flexural stiffness were obtained from the axial stress – strain relationship measured by the load cell and strain gauges during the quasi-static tests of the first S-FSC specimens. The second S-FSC specimen was not extended past yield in the quasi-static test. Finally, the yield moment in positive and negative bending was calculated using the properties obtained from the coupon test on the copper alloy material test. The yield moment was obtained by multiplying the section modulus times the yield stress. The mass of each beam element, although irrelevant for the modeling of quasi-static tests, was based on the density and geometry of the cooper alloy flexible strap.

Table 4.1 S-FSC Properties for RUAUMOKO Model

Elastic Modulus (ksi)	1.41×10^{7}
Shear Modulus (ksi)	5.40×10^{6}
Cross-Sectional Area (in^2)	2.25
Moment of Inertia (in^4)	2.93×10^{-3}
Weight/Unit Length (lbs/ft)	0.72
Bi-Linear Factor	0.365
Yield Moment (lbs-in)	1266

To model the quasi-static test conducted on the improved bus slider, a simple bi-linear axial element was constructed based on the load-displacement response obtained during the test. The resulting properties of this axial element are presented in Table 4.2.

Table 4.2 New Bus Slider Properties for RUAUMOKO Model

Spring Stiffness (lbs/in)	1400
Bi-Linear Factor	0.0255
Equivalent Yield Force (lbs)	67

4.2.2 LOADING FUNCTION

To approximate the loading protocol used in the quasi-static tests, one full cycle of slowly applied dynamic loading was considered as the loading function in the numerical model. This was accomplished using the shape function feature in RUAUMOKO. By using the shape function, a maximum load can be reached at a given loading increment expressed in terms of a ratio to the maximum load specified. Through this procedure, a ratio of 0.0 is 0 lbs, and a ratio of 1.0 is the load that is assigned in the shape function. Utilizing this method, the models were subjected to a protocol of 0.0, 1.0, 0.0, -1.0, 0.0, thereby completing one full loading cycle. The time history of this cycle is shown in Figure 4.2. The loading increment assigned to the analysis was an interval of 10 seconds. This was chosen such that the test would be slow and could be monitored, and also because this interval is much longer than the natural period of vibration of the specimen, which was 0.211 seconds.

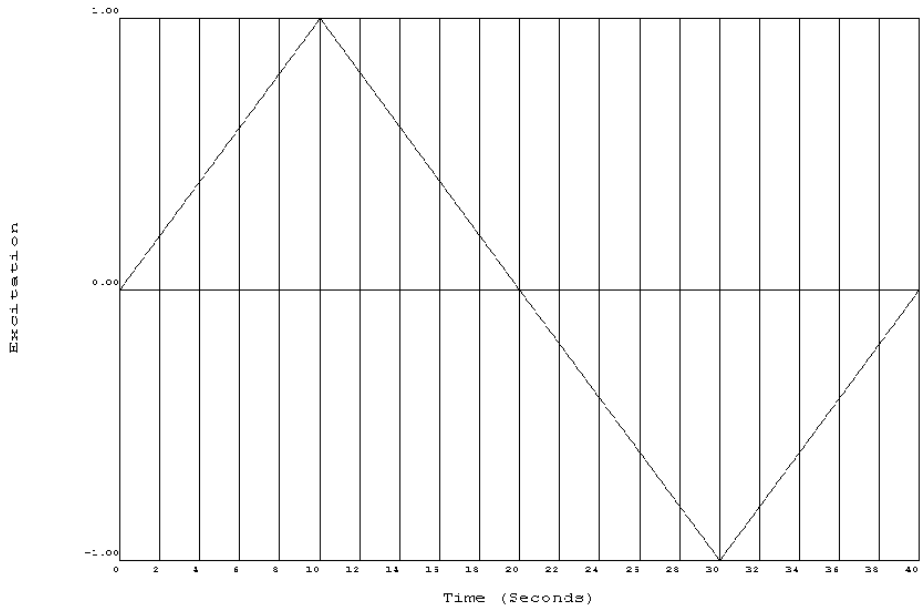

Figure 4.2 Loading Function Used in Numerical Model

4.2.3 PREDICTIONS OF QUASI-STATIC TESTS

The load-displacement predictions of the numerical models were compared with the hysteresis loops obtained experimentally for each respective connector. For the S-FSC specimen, the comparison of the initial stiffness illustrates a good match, as shown in Figure 4.3. For the purpose of predicting the non-linear behavior of the S-FSC specimen, a maximum load of 180 lbs was specified. The model predicts that the S-FSC specimen would start yielding at displacement of approximately of 4 in corresponding to a load of just over 150 lbs.

Figure 4.4 compares the load-displacement hysteresis loop resulting from the bi-linear axial model of the improved bus slider against the experimental results obtained during the quasi-static test. Since the model was derived directly from the experimental results, its predictions are very good.

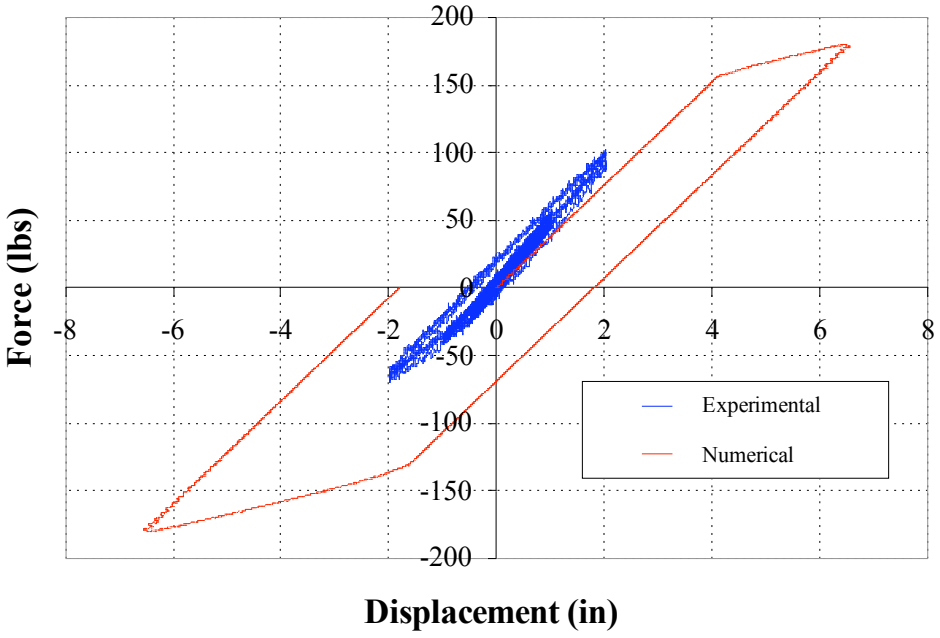

Figure 4.3 S-FSC Hysteresis Loops

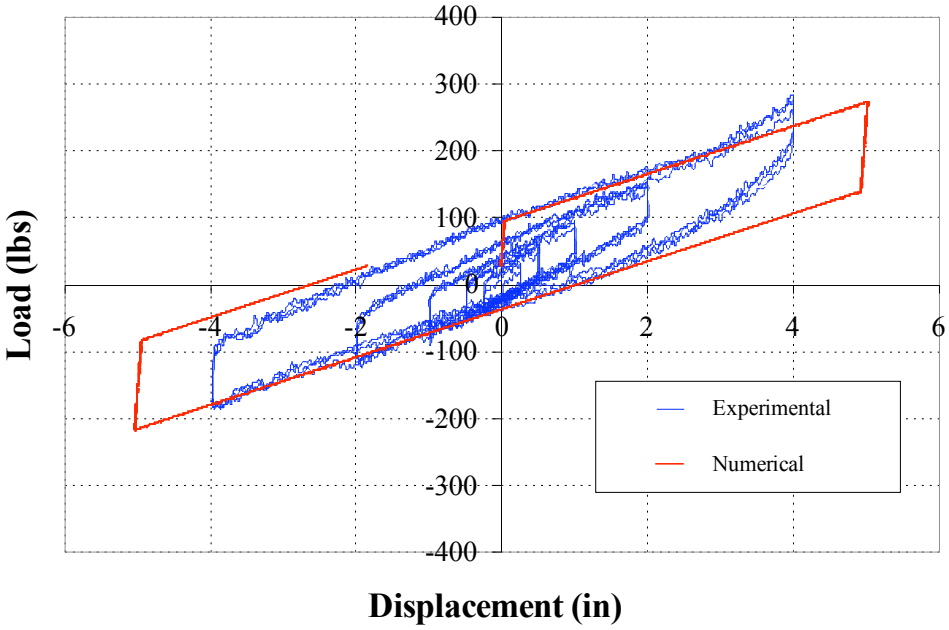

Figure 4.4 Improved Bus Slider Hysteresis Loops

4.3 MODELING OF SEISMIC TESTS

4.3.1 PREDICTIONS OF UNCOUPLED TEST RESULTS

The first step in modeling the complete shake table tests was to construct models for the five different equipment pairs in RUAUMOKO. Each equipment model included ten beam-column elements totaling a length of 14 ft. Each was assigned a linear-elastic behavior in flexural and axial deformations based on elastic section properties. The last element at the top of each equipment item was assigned a rigid end since the lumped weights would be placed in this region. Additionally, the appropriate weight for each equipment was added to the top node. The final component of the models was rotational springs at their base nodes to account for the slight rocking at the base of the equipment items. With the addition of these springs, natural frequencies matching well with the measured frequencies were obtained. The rotational stiffness of these springs is presented for each equipment item in Table 4.3.

Table 4.3 Rotational Spring Stiffness of Equipment

Equipment #	Rotational Spring Stiffness (in-lbs/rad)
1	11097000
2	290877000
3	110020000
4	1371320000
5	1371320000

For each equipment item model, an initial stiffness Rayleigh Damping model was incorporated. Two damping ratios were applied to the first two modes of vibration of each system. In the case of the shake table simulations, the first two modes were the first mode of each equipment item. To determine the damping ratio values of each of

the equipment items, the data from the damping evaluation tests were used. First, the displacement time-histories were examined to determine the maximum displacement value for each test with each ground motion. Then, this displacement value was used in the damping plots of Appendix D to determine the corresponding damping ratio. The equivalent viscous damping values used to simulate the uncoupled tests are tabulated in Table 4.4.

Table 4.4 Equipment Damping Ratios for Uncoupled Tests

Equipment #	Damping Ratios (%)		
	Newhall 30%	Tabas 25%	Tabas 50%
1	0.432	0.429	0.425
2	0.122	0.001	0.001
3	0.051	0.001	0.001
4	0.423	0.469	0.496
5	0.499	0.400	0.351

After the correct frequencies and damping ratios were achieved for the equipment items, the models were then subjected to the ground motions. For consistency, each ground motion used in the RUAUMOKO model was the actual acceleration data obtained from the accelerometer connected to the shake table (Instrument A1) for each respective test. The ground motions used for these tests were Newhall 30%, Tabas 25%, and Tabas 50%.

For each test, four time-histories were predicted by the numerical models and compared against the experimental results:

- Relative Displacement at the top of Equipment A
- Relative Displacement at the top of Equipment B
- Absolute Acceleration at the top of Equipment A
- Absolute Acceleration at the top of Equipment B

Figure 4.5 compares the predictions of the uncoupled Equipment Pair 2 model under the Newhall ground motion at 30% span against the experimental results. It is clear from the figure that the predictions compare very well with the experimental results. It must be noted, however, that in the model, a single equivalent viscous damping ratio can only be applied to the equipment items. In reality, as shown by the damping evaluation test data, the damping ratio is a function of the amplitude of the response. Consequently, the numerical results for the seismic data may exhibit slight differences at smaller displacement and acceleration amplitudes. Table 4.5 compares the numerical and experimental maximum values of displacements and accelerations for the uncoupled Equipment Pair 2 under all earthquake ground motions considered. Despite that the model can not capture the variation of equivalent viscous damping with response amplitude, the peak predictions of the model agree reasonably well with the measured peak values.

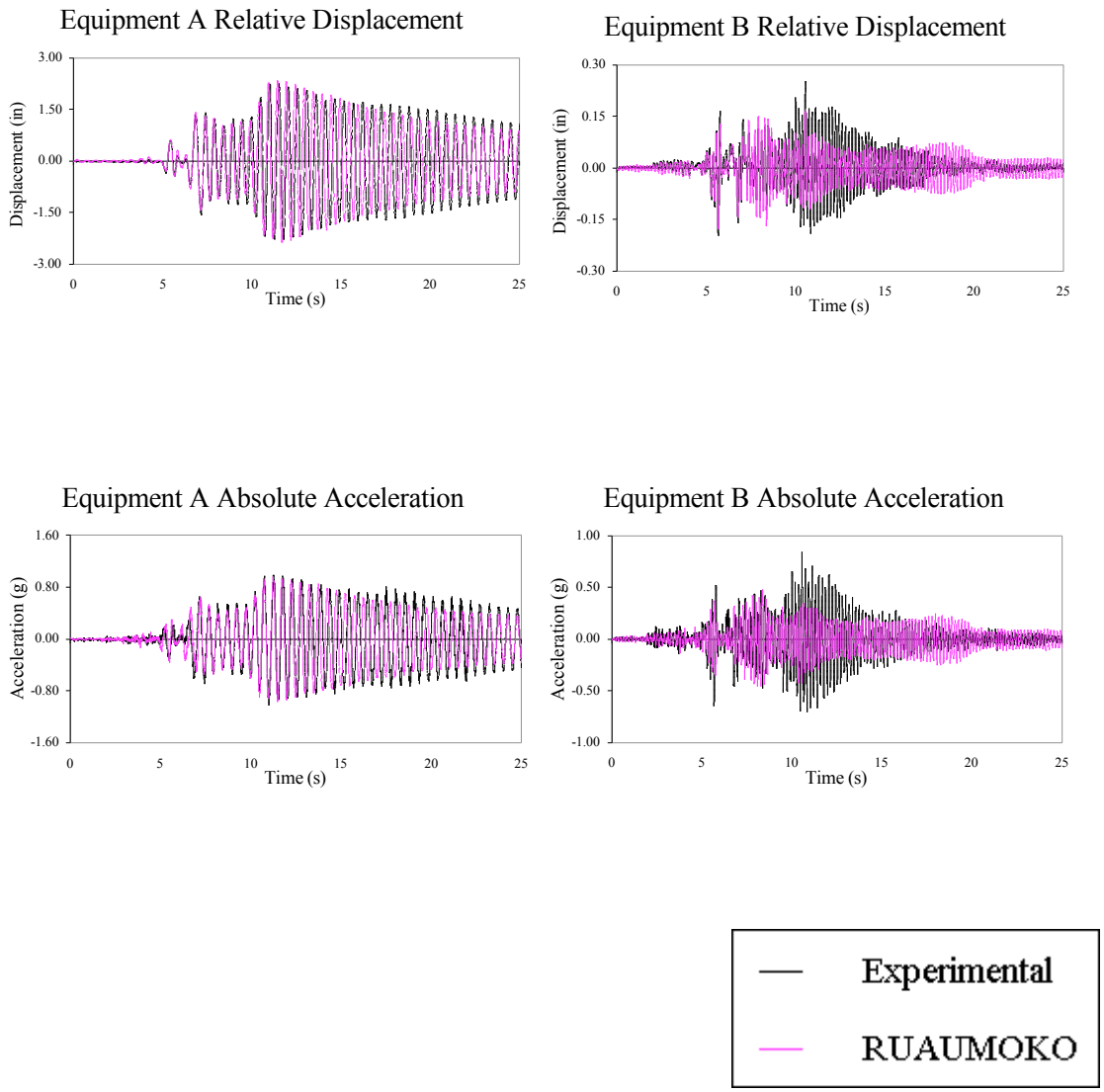

Figure 4.5 Time-History Comparison for Uncoupled Equipment Pair 2, Newhall 30%

Table 4.5 Maximum Displacements and Accelerations for Uncoupled Equipment Pair 2

Ground Motion-Span (%)	Experimental Displacement Equipment A (in)	RUAUMOKO Displacement Equipment A (in)	Experimental Acceleration Equipment A (in)	RUAUMOKO Acceleration Equipment A (in)
Newhall 30%	2.27	2.36	1.02	0.96
Tabas 25%	3.01	3.06	1.26	1.30
Tabas 50%	4.60	5.70	1.92	2.33

Ground Motion-Span (%)	Experimental Displacement Equipment B (in)	RUAUMOKO Displacement Equipment B (in)	Experimental Acceleration Equipment B (in)	RUAUMOKO Acceleration Equipment B (in)
Newhall 30%	0.25	0.18	0.84	0.48
Tabas 25%	0.48	0.41	1.79	1.24
Tabas 50%	0.71	0.68	2.85	2.21

4.3.2 PREDICTIONS OF S-FSC COUPLED TEST RESULTS

The numerical models of the equipment interconnected by the S-FSC specimen were similar to that of the uncoupled equipment. The properties and geometry of the equipment items remained unchanged. The S-FSC rigid bus assembly was modeled by a single axial spring element with the properties shown in Table 4.6. These properties were extracted from the load-displacement hysteretic behavior predicted by the model of the quasi-static test on the S-FSC specimen shown in Figure 4.3 Figure 4.6 shows the geometry of the interconnected numerical model.

Table 4.6 Properties of Axial Spring Element Modeling the S-FSC Specimen

Spring Stiffness (lbs/in)	38.05
Bi-Linear Factor	0.365
Yield Load (lbs)	157

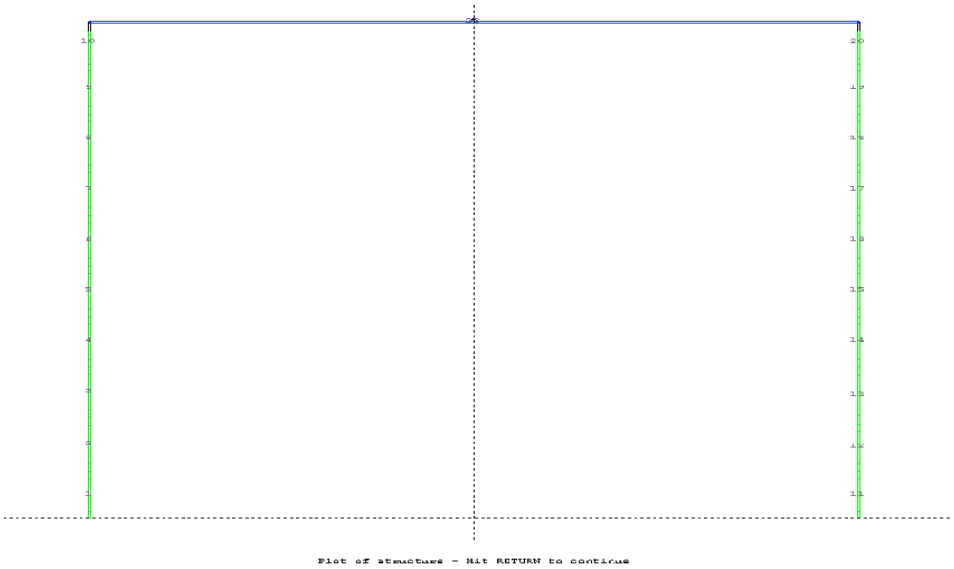

Figure 4.6 Geometry of Interconnected Model

The accuracy of the coupled numerical modeling was first assessed by comparing the predicted natural frequencies with the measured natural frequencies. This comparison is presented in Table 4.7 for Equipment Pair 2. Clearly the frequencies match well, showing that the numerical model is able to predict accurately the dynamic properties of the coupled equipment items.

Table 4.7 Numerical and Experimental Frequencies for Equipment Pair 2 Interconnected with S-FSC Specimen

	Equipment A	Equipment B
Experimental Coupled Frequency (Hz)	2.109	5.195
Numerical Coupled Frequency (Hz)	2.052	5.424

The coupled models incorporating the S-FSC specimen were subjected to the aforementioned three earthquakes, Newhall 30%, Tabas 25% and Tabas 50%. The experimental and predicted peak displacements and accelerations for Equipment pair 2 are compared in Table 4.8, while the complete displacement and acceleration time-histories are presented in Figure 4.7 for the Newhall ground motion at 30% span. Again, the numerical predictions match the numerical results reasonably well.

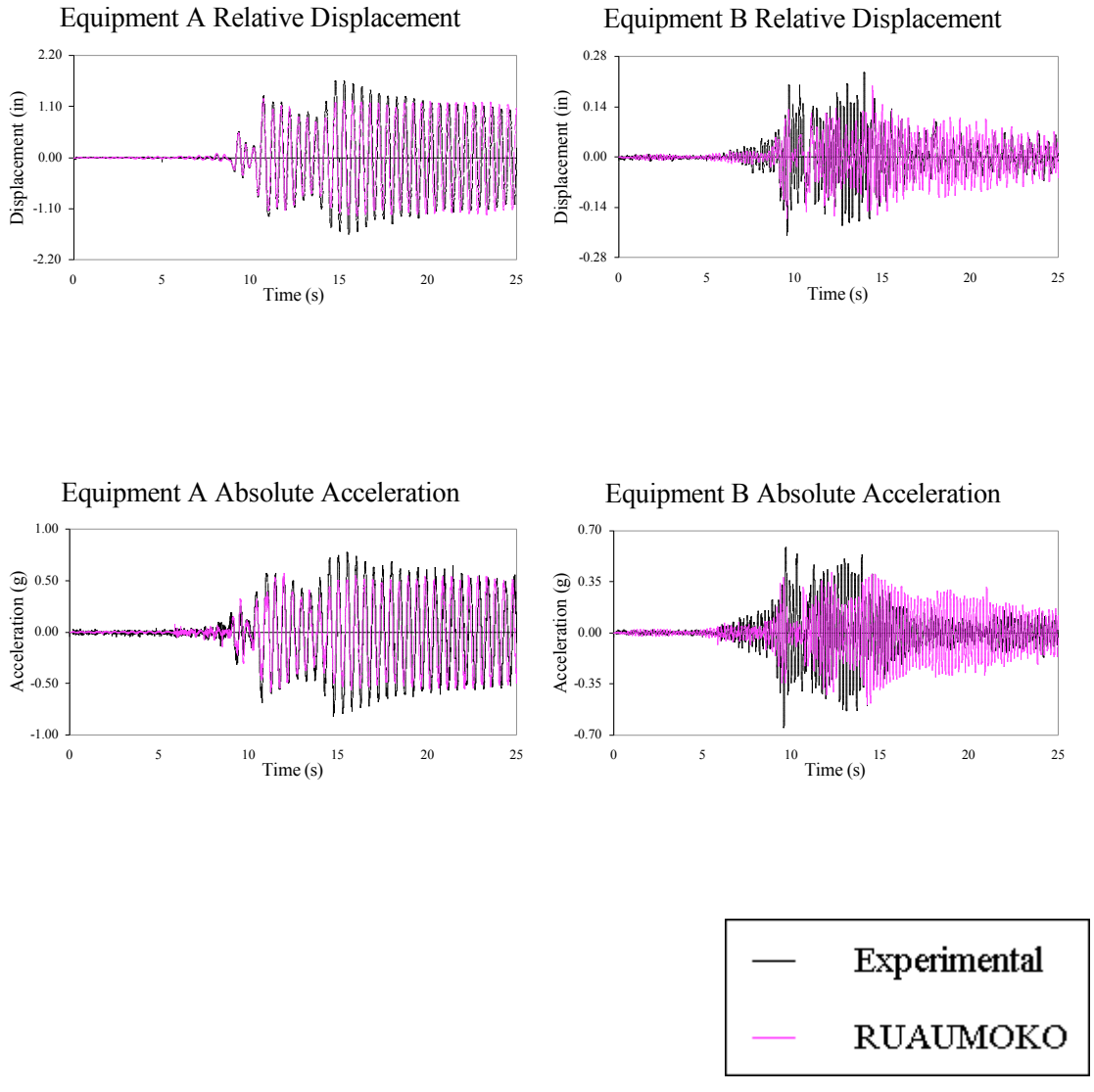

Figure 4.7 Time-History Comparison for S-FSC Test, Equipment Pair 2, Newhall 30%

Table 4.8 Maximum Displacements and Accelerations for S-FSC Tests for Equipment A and B

Ground Motion-Span (%)	Experimental Displacement Equipment A (in)	RUAUMOKO Displacement Equipment A (in)	Experimental Acceleration Equipment A (in)	RUAUMOKO Acceleration Equipment A (in)
Newhall 30%	1.65	1.27	0.82	0.58
Tabas 25%	2.35	2.37	1.10	1.08
Tabas 50%	4.56	4.34	1.95	1.99

Ground Motion-Span (%)	Experimental Displacement Equipment B (in)	RUAUMOKO Displacement Equipment B (in)	Experimental Acceleration Equipment B (in)	RUAUMOKO Acceleration Equipment B (in)
Newhall 30%	0.24	0.20	0.65	0.49
Tabas 25%	0.43	0.49	1.06	1.58
Tabas 50%	0.73	0.93	2.38	3.03

4.3.3 PREDICTIONS OF IMPROVED BUS SLIDER COUPLED TEST RESULTS

The numerical models of the equipment interconnected by the improved bus slider were similar to that of the equipment interconnected with the S-FSC specimen. Only the properties of the axial spring connecting the two equipment models we modified to represent the hysteretic behavior of the improved bus slider. These properties are listed in Table 4.2.

Again the accuracy of the coupled numerical model was first assessed by comparing the predicted natural frequencies with the measured natural frequencies. This comparison is presented in Table 4.9 for Equipment Pair 2. It can be seen that the model significantly over-predicts the measured natural frequencies. This over-prediction can be explained by the fact that during the test, the bus slider was sliding under the white noise excitation, thereby reducing the axial stiffness of the connecting

bus slider. The numerical model, on the other hand, computed the natural frequencies based on the initial lateral stiffness of the spring element before sliding was initiated.

Table 4.9 RUAUMOKO and Experimental Frequencies with New Bus Slider Assembly for Equipment Pair 2

	Equipment A	Equipment B
Experimental Coupled Frequency (Hz)	2.578	5.273
RUAUMOKO Coupled Frequency (Hz)	3.910	8.015

The coupled models incorporating the improved bus slider connector were also subjected to the Newhall 30%, Tabas 25% and Tabas 50% ground motions. The experimental and predicted displacements and accelerations time-histories for Equipment Pair 2 are compared Figure 4.8 for the Newhall ground motion at 30% span. Significant differences can be observed between the predictions of the numerical model and the experimental results. The model signigicantly under-predicts the response of the more flexible Equipment A. By looking at the details of the time-histories for Equipment A, it can be seen that the model predicts the phase of the response reasonably well; only the amplitudes are under-predicted.

In order to match the experimental results better, a parametric study was undertaken on the properties of the connecting axial spring representing the improved bus slider. A very good correlation between the experimental and numerical predictions was achieved when the effective yield load of the spring element, representing the slip load of the bus slider, was reduced from its measured value of 67 lbs to 10 lbs, as shown in

Figure 4.9 and Table 4.10. This result suggests that the frictional characteristics of the bus slider installed in an horizontal position between interconnected equipment might be lower than that in the vertical position in which it was tested. More studies are required, however, to confirm this phenomenon.

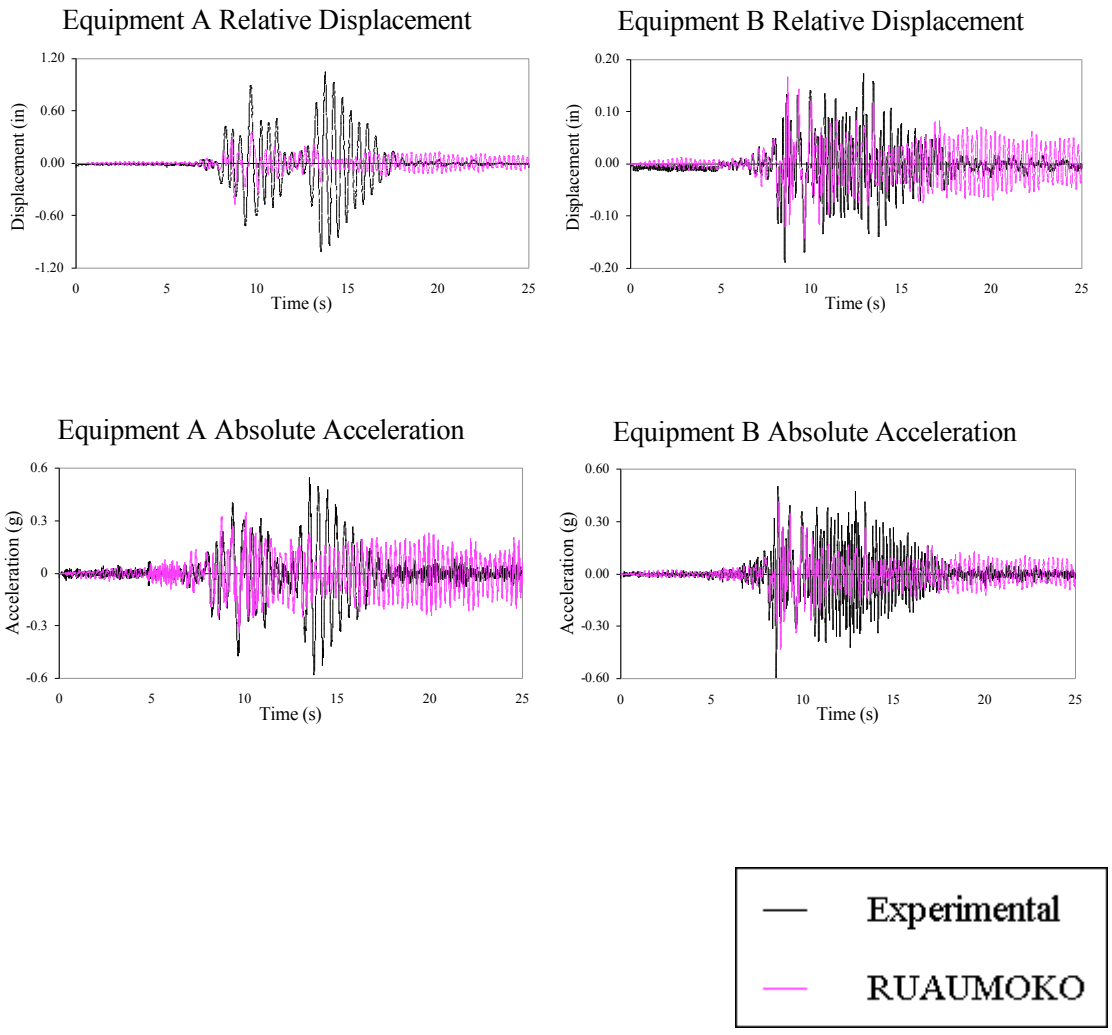

Figure 4.8 Time-History Comparison for Bus Slider Test, Equipment Pair 2, Newhall 30%

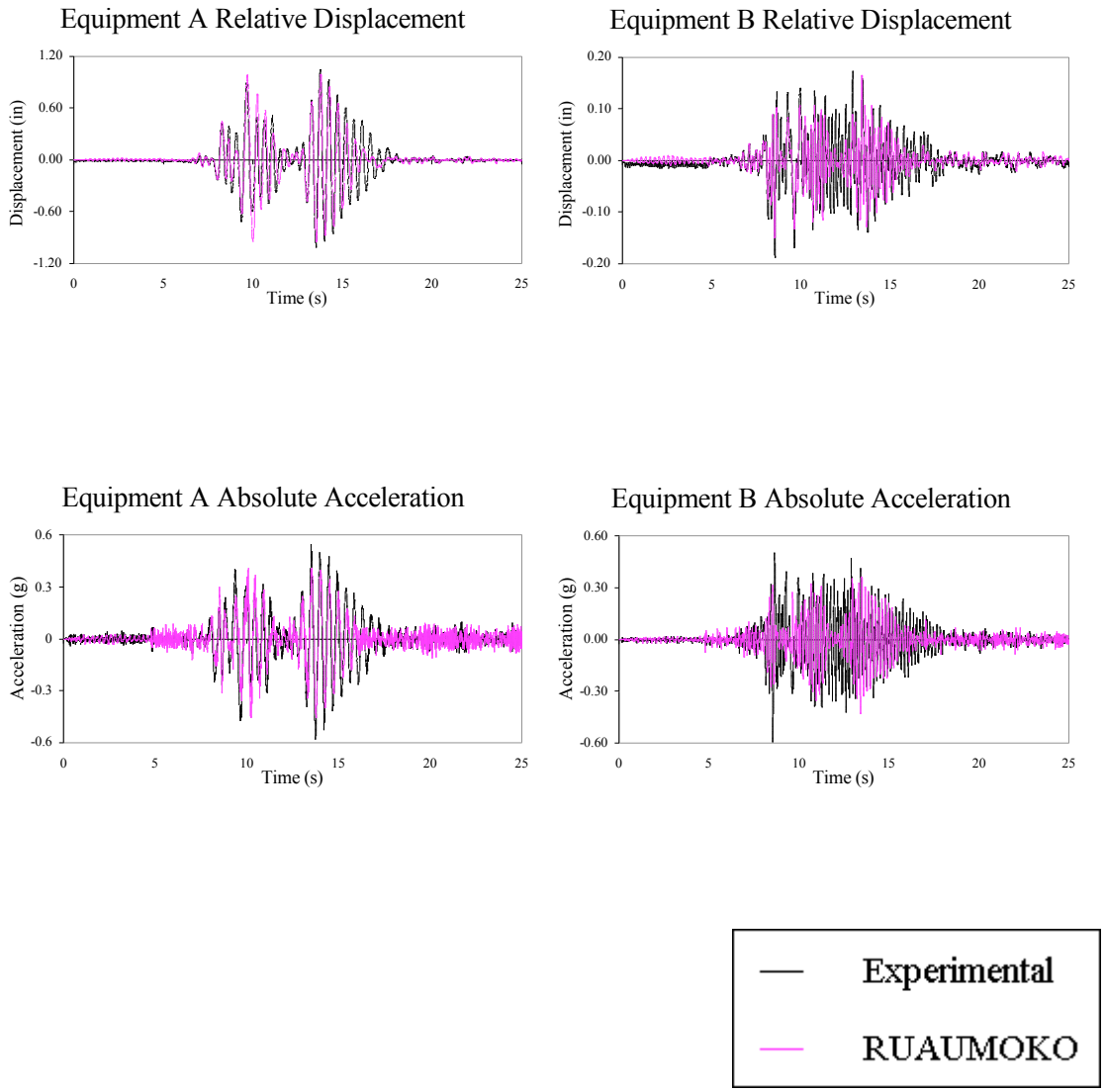

Figure 4.9 Time-History Comparison for Bus Slider Test for 10 lbs Slip Load, Equipment Pair 2, Newhall 30%

Table 4.10 Maximum Displacements and Accelerations for New Bus Slider Tests for Equipment A and B, Slip Load of Bus Slider Reduced to 10 lbs

Ground Motion-Span (%)	Experimental Displacement Equipment A (in)	RUAUMOKO Displacement Equipment A (in)	Experimental Acceleration Equipment A (in)	RUAUMOKO Acceleration Equipment A (in)
Newhall 30%	1.05	1.00	0.58	0.45
Tabas 25%	1.73	1.76	0.89	0.85
Tabas 50%	3.62	3.96	2.05	1.84

Ground Motion-Span (%)	Experimental Displacement Equipment B (in)	RUAUMOKO Displacement Equipment B (in)	Experimental Acceleration Equipment B (in)	RUAUMOKO Acceleration Equipment B (in)
Newhall 30%	0.19	0.17	0.59	0.43
Tabas 25%	0.34	0.36	1.15	1.06
Tabas 50%	0.70	0.65	2.23	2.07

5. CONCLUSIONS

The quasi-static and shake table tests performed in this project has provided an opportunity to evaluate the interactions between components of substation equipment connected by improved rigid bus connectors. The tests have also provided data for a current PEER-PG&E analytical project.

Based on the results of the quasi-static tests performed on the improved rigid bus connectors, the following conclusions can be drawn:

- The first (mis-shaped) S-FSC specimen tested exhibited large and stable hysteresis loops with good energy dissipation capabilities. The second S-FSC specimen incorporating the correct initial geometry was not tested past the yield limit, but can be assumed to exhibit nearly the same behavior as the mis-shaped S-FSC since both specimens exhibited the same initial stiffness.
- The initial stiffness of the S-FSC was nearly the same as the initial stiffness of FSC 30-2023, and approximately one-seventh the initial stiffness of FSC 30-2021 and FSC 30-2022
- The equivalent damping ratios of all FSC specimens increase with displacement amplitude, indicating higher dissipation capacity at large inelastic displacements. FSC 30-2021 and FSC 30-2022 exhibit damping ratios significantly higher than the more flexible FSC 30-2023 for the complete range of displacement amplitudes considered in the test.

- The first (mis-shaped) S-FSC specimen exhibited higher damping than all the original FSC specimens due to the friction of the strands in the looped regions. The second S-FSC exhibited the lowest damping.
- The new bus slider was not completely centered and was compressed by 3 in to accommodate a stroke of 5 in for both loading directions.
- Both the old and new bus sliders exhibited a behavior that is typical of a Coulomb-type friction system coupled with an elastic restoring force mechanism.
- The improved bus slider had a post-slip stiffness of 44 lbs/in, while the original bus slider had a stiffness of 89 lbs/in, nearly twice the stiffness.

Based on the results of the shake table tests performed on five different pairs of generic equipment connected by three different types of rigid bus connectors, the following conclusions can be drawn:

- The natural frequencies measured on the generic equipment specimens interconnected by the bus assemblies were always between the natural frequencies obtained for the uncoupled equipment specimens. The coupling effect from the new bus slider specimen displayed this phenomenon the most.
- The natural frequencies measured on the generic equipment specimens interconnected by the SEFCOR connector were nearly the same as the frequencies obtained from the uncoupled equipment specimens.

- The bus slider specimen exhibited the highest damping capabilities of the three specimens.
- The new bus slider specimen performed well except when subjected to the high amplitude Tabas record, when the plunger extended to the point where the stoppers hit the inside of the tube, and high impact forces were transmitted to the equipment items. More stroke may be needed to prevent this impact phenomenon.
- The response of the equipment items connected with the SEFCOR connector was similar to the response with the S-FSC specimen. The size of the loops from the SEFCOR specimen is believed to be great enough such that the connector will not become taut under severe ground motions.
- Among the three connectors investigated, the new bus slider consistently reduced the response at the top of both equipment specimens.

Based on the numerical modeling of the quasi-static and shake table tests using the RUAUMOKO computer program, the following conclusions can be made:

- The hysteresis loops from quasi-static modeling of both the S-FSC and new bus slider specimens were shown to match the experimental results well.
- The response at the top of both equipment items in the model for the S-FSC matched well with the response from the experimental results.
- The model under-predicted the response of the lower frequency equipment when interconnected with the bus slider. Good agreement was achieved when

the slip load of the connecting spring element, representing the bus slider, was reduced from 67 lbs to 10 lbs. This results suggest that the frictional characteristics of the bus slider might be different in the horizontal and vertical positions.

6. REFERENCES

Abrahamson, N. (1997). Personal Communication.

Applied Technology Council (1992). "Guidelines for Cyclic Seismic Testing of Components of Steel Structures", ATC-24, Redwood City, CA.

Benuska, L., Technical Editor (1990). "Loma Prieta Earthquake Reconnaissance Report", Earthquake Spectra, Supplement to Volume 6, Earthquake Engineering Research Institute, Oakland, CA.

Carr, A.J. 2000. RUAUMOKO – inelastic dynamic analysis program. Department of Civil Engineering, University of Canterbury, Christchurch, New Zealand.

Clough, R.W., and Penzien, J. (1993). "Dynamics of Structures", Second Edition, McGraw-Hill, New York.

Der Kiureghian, A., Sackman, J.L., and Hong, K.J. (1999). "Interaction in Interconnected Electrical Substation Equipment Subjected to Earthquake Ground Motions", Report PEER 1999/01, Pacific Earthquake Engineering Research Center, University of California, Berkeley, Berkeley, CA.

Experimental Dynamic Investigations. (1993). "U2 & V2 Manual", Vancouver, Canada

Filiatrault, A., Tremblay, R., Thoen, B.K. and Rood, J. (1996). "A Second Generation Earthquake Simulation System in Canada: Description and Performance Evaluation", 11th World Conference on Earthquake Engineering, Acapulco, Mexico, Paper #1204 on CD ROM.

Filiatrault, A., Kremmidas, S., Elgamal, A. and Seible, F. (1999). "Substation Equipment – Rigid and Flexible Conductor Studies", Structural Systems Research Project Report No. SSRP-99/09, Department of Structural Engineering, University of California, San Diego, La Jolla, CA, 218 p.

Filiatrault, A. and Kremmidas, S. (2000)."Seismic Interaction Between Components of Electrical Substation Equipment Interconnected by Rigid Bus Conductors", ASCE Journal of Structural Engineering, 126(10), 1140-1149.

Filiatrault, A., Kremmidas, S., Seible, F., Clark, A.J., Nowak, R., and Thoen, B.K. (2000). "Upgrade of First Generation Uniaxial Seismic Simulation System with Second Generation Real-Time Three-Variable Digital Control System", 12th World Conference on Earthquake Engineering, Auckland, New Zealand, Paper No. 1674, on CD-ROM.

Filiatrault, A., and Stearns, C. (2003). "Electrical Substation Equipment Interaction - Experimental Flexible Conductor Studies", Structural Systems Research Project Report No. SSRP-2002/09, Department of Structural Engineering, University of California, San Diego, La Jolla, CA, 389 p.

Hall, J., Technical Editor (1995). "Northridge Earthquake of January 17, 1994 Reconnaissance Report Volume 1 ", Earthquake Spectra, Supplement to Volume 11, Earthquake Engineering Research Institute, Oakland, CA.

Institute of Electrical and Electronics Engineers. 1997. "Recommended Practices for Seismic Design of Substations", IEEE-693 Standard, IEEE Standards Dept., Piscataway, NJ.

Song, J. 2004. "Seismic Response and Reliability of Electrical Substation Equipment and System," Ph.D. Thesis, University of California, Berkely, CA.

Song, J., Der Kiureghian, A., and Sackman, J.L. 2004. „Reliability of Electrical Substation Equipment Connected by Rigid Bus," Proceedings of the 13th World Conference on Earthquake Engineering, Vancouver, Canada.